FRAGMENTATION OF QUARKS AND GLUONS, TESTS OF QCD IN e^+e^- ANNIHILATION*

Jonathan Dorfan

Stanford Linear Accelerator Center
Stanford University, Stanford, California 94305

TABLE OF CONTENTS

---

1. INTRODUCTION

This report covers the topics of fragmentation of quarks and gluons and tests of QCD in e^+e^- annihilation and is a summary of a rapporteur talk given at the 1983 International Symposium on Lepton and Photon Interactions at High Energies. The speaker was provided with an overwhelming amount of material for this talk and has been unable to incorporate it all in this report if only because of space limitations. Apologies are offered ahead of time to the people whose work is not represented here. We recommend that the interested reader consult the list of contributed papers which appear in the proceedings.

The topics which are covered in Section 2 are new data on the general characteristics of the e^+e^- environment at the Υ and and at PETRA and PEP. For the first time there is a lot of data on resonance production — η, K^*, ρ, ϕ, Ξ. There is more data on c quark fragmentation from tagged $D^{*\pm}$ and direct observation of D^+ and D^o. There are four experiments using high P_t leptons to measure the b quark fragmentation function — agreement amongst the experiments is very good. All these measurements can usefully be incorporated in the Monte Carlo simulation models.

Section 3 covers the general area of QCD tests. α_s has been measured using the energy dependence of the total hadronic cross section. Unfortunately this method is not very precise. Other measurements of α_s from shape analyses and energy-energy correlations have been done including the effects of all second order QCD diagrams. The results seem to depend both on the procedure and the models used to extract α_s. The evidence for differences in gluon and quark fragmentation are reviewed. There is now evidence that baryon conservation occurs locally in a jet rather than globally in an event. Multiplicity and jet mass correlations are presented as well as data on KNO scaling.

2. STUDY OF THE HADRONIC FINAL STATES; PARTICLE PRODUCTION YIELDS AND QUARK FRAGMENTATION

In this section we will cover the composition of e^+e^- hadronic final states. Particle yields will be given as well as information concerning the fragmentation functions of charm and bottom quarks. There are now measurements of the yields of a wide range of resonant states. The selection of hadronic events in the analyses described in this section follows a standard prescription which includes cuts on total charged particle multiplicity and detected energy. The exact cuts will not be discussed for each set of data presented — suffice it to say that the backgrounds to the hadronic samples are in all cases small and in no way affect the validity of the conclusions.

(a) Measurements of the Relative Yields of $\pi^{\pm}$, $K^{\pm}$ and Protons at PEP and PETRA

The TASSO experiment[1] published results on the relative yields of charged pions, kaons and protons at a center-of-mass energy ($\sqrt{s}$) of 34 GeV. New data are now available at 29 GeV from the PEP experiments TPC[2] and DELCO.[3] The performance of the TPC dE/dx system has matured to the point where they achieve a resolution $\sigma = 3.6\%$ for charged particles in hadronic jets. Their dE/dx performance is shown in Fig. 1 and the resulting particle separation is shown in Fig. 2. Using the dE/dx measurements the relative numbers of charged pions, kaons and protons were obtained in the range 0.3 GeV/c to 6 GeV/c. Below 1 GeV/c the separation is excellent and one simply counts tracks in the three particle dE/dx bands (a small correction for the electron/kaon overlap is made). Above 1 GeV/c a statistical separation was made. For a given momentum bin, a fit was made to the sum of four Gaussians (pions, kaons, protons and electrons) whose relative positions and widths were fixed. The data are shown in Fig. 3 — the errors include the contribution from systematic effects and the effects of correlations in the variables used in the fit. The TPC data are compared with those of TASSO and the agreement is good. The data have been corrected for detector inefficiencies to yield inclusive production cross sections as given in Fig. 4. The cross section is plotted in terms of the scaling variable $x = 2E/\sqrt{s}$, where E is the particle energy, and has been normalized to the measured hadronic cross section. Figure 3 indicates that at low particle momenta pions dominate the hadronic yield. This is presumably due to the low mass of pions relative to kaons and protons. As one moves towards the maximum available momentum one is studying leading particles. The pion and

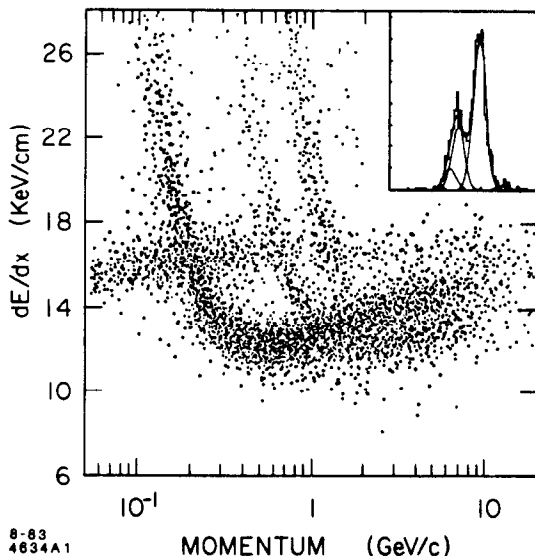Fig. 1. TPC dE/dx versus momentum for the 1983 sample of hadronic events. Only tracks with more than 120 wires are included. The insert shows the ratio of measured dE/dx to the expected dE/dx for pions, for momenta between 3.5 and 6 GeV/c. The solid lines represent the contributions of electrons, pions, kaons and protons. The proton signal is a 5 standard deviation effect at the present statistics (29.2 pb^{-1}).
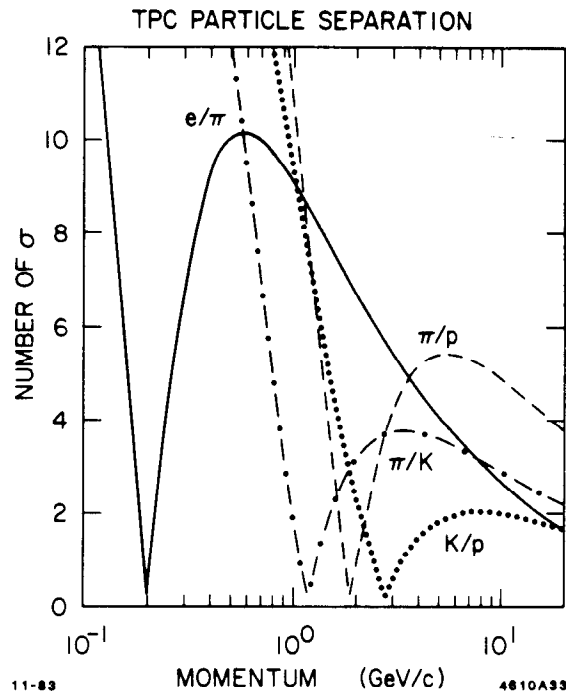
TPC PARTICLE SEPARATION

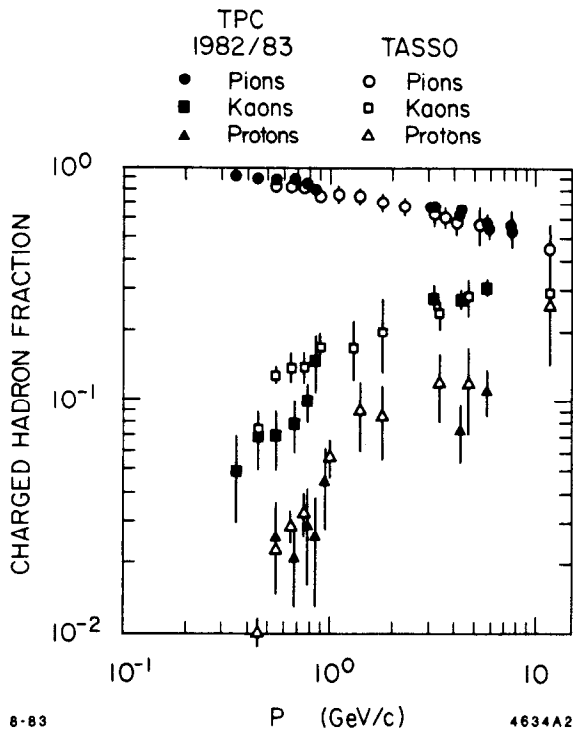Fig. 2. Particle separation for the TPC with $\sigma = 3.6\%$.

Fig. 3. Particle fractions versus momentum for pions, kaons, and protons, for the TPC (preliminary) and the TASSO experiments. TPC points for momenta below 1 GeV/c are from 3.8 pb^{-1}, and from 29.2 pb^{-1} otherwise. The systematic uncertainties are included in the error bars.

4

kaon yields become comparable but the proton yield is suppressed because one pays a price for pulling a diquark system out of the vacuum. From Fig. 4 we see that the particle production slopes for the three particle species are similar which would indicate similar production mechanisms. However it should be remembered that the issue is complicated by the fact that most of the stable hadrons observed result from the decay of resonances. Using Monte Carlo simulation programs, which account well for the hadronic final states, the TPC group is able to obtain the probability of producing an $s\bar{s}$ quark pair relative to a $u\bar{u}$ quark pair in the process whereby a quark cascades into hadrons. From the data shown in Fig. 4 the TPC group finds this relative probability to be $P(s\bar{s})/P(u\bar{u}) = 0.26 \pm 0.1$. The error includes the uncertainties in the models arising from the shapes of the fragmentation functions, decay branching fractions and the ratio of vector to scalar production.

Figure 5 shows the charged particle fractions as measured by the DELCO group. In all cases a statistical unfold method is used. For tracks with momenta below 2 GeV/c, time of flight measurements were used to effect a separation, while for momenta above 2.6 GeV/c, the separation of
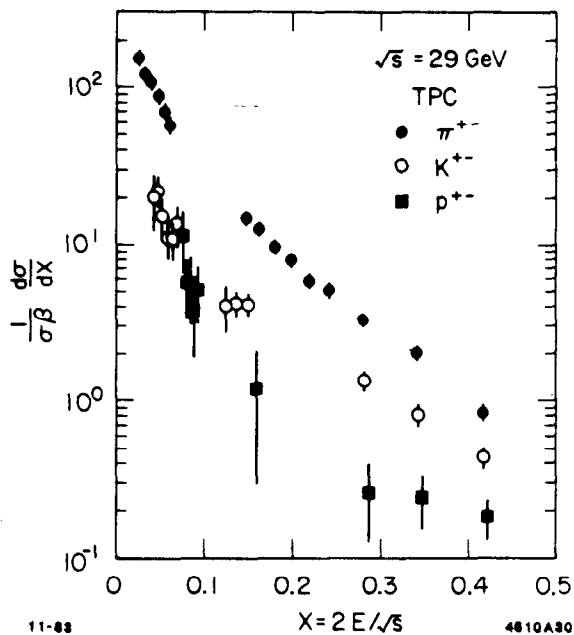

Fig. 4. Preliminary differential cross section versus X (hadron energy/beam energy) at a center-of-mass energy of 29 GeV, for pions, kaons and protons.
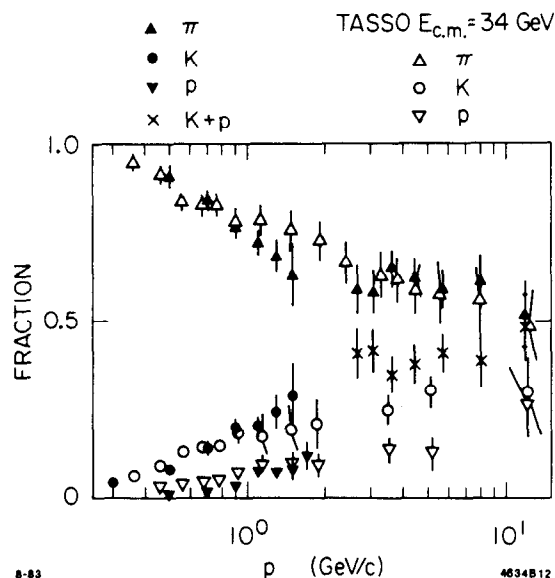

Fig. 5. Particle fractions versus momentum as measured by the DELCO group.

pions from kaons and protons come from the Cerenkov counters. The DELCO data are in reasonable agreement with the data of TPC and TASSO and confirm the trends and implications discussed earlier in this section.

(b) Measurements of π^o and η Production

There are new results on π^o production from the CELLO group[4] and the TPC group. CELLO has made measurements at $\sqrt{s} = 14$, 22 and 34 GeV, with corresponding integrated luminosities of 1.1 pb^{-1}, 2.5 pb^{-1} and 7.9 pb^{-1}. The π^o's were reconstructed from photons measured in the CELLO liquid argon calorimeters. Reconstructing π^o's in the crowded jet environment presents many experimental difficulties[4] — the complexity of which is too detailed for this discussion. Instead we show in Fig. 6 the photon-photon invariant mass spectrum for the three center-of-mass energies studied. Clear π^o peaks can be seen. A background subtracted, inclusive cross section for π^o's is shown in Fig. 7 along with the data of the Lead Glass Wall[5] experiment which span the energy region from 4.9-7.4 GeV. The CELLO group has compared their π^o yields with the TASSO yields for charged pions and obtain a ratio $2\pi^o/(\pi^+ + \pi^-)$ of 1.21 ± 0.42, 0.96 ± 0.40 and 1.01 ± 0.35 at $\sqrt{s} = 14$, 22 and 34 GeV respectively. Hence within statistics the π^o's have the same production characteristics as the charged pions. There is a tendency for the CELLO π^o data to indicate scaling violations at the 1.5σ level. However these effects could be due to nonperturbative effects which, at these energies, are capable of explaining the apparent scaling violations.
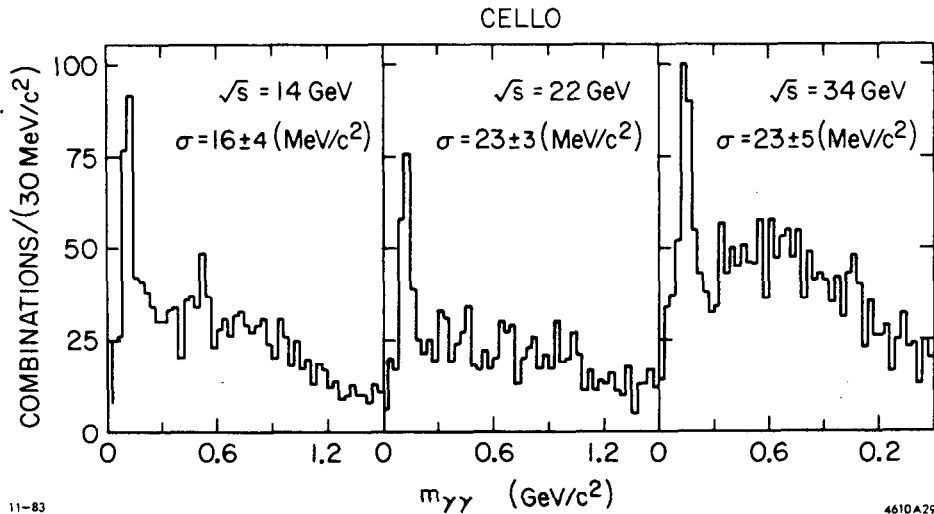

Fig. 6. Photon-Photon invariant mass spectra as measured by the CELLO collaboration.

6

Figure 8 shows the photon-photon invariant mass spectrum from the TPC detector.[2] The data set comprises 29 pb^{-1} at $\sqrt{s} =$ 29 GeV. Following a background subtraction and corrections for detector inefficiencies, an inclusive cross section is obtained as shown in Fig. 9. Also shown are the 34 GeV data from TASSO[6] and CELLO. The TPC errors include a 15% contribution for systematics. Agreement among the three experiments is fair. Figure 10 compares the inclusive cross sections for TPC charged and neutral pions which strongly suggest that the production mechanisms are the same.

The JADE group[7] has made the first observation of η's in the 30 GeV energy region. Details

Fig. 7. Inclusive cross sections as measured by CELLO and the LGW experiment.

of the JADE experiment and the lead glass electromagnetic calorimeters can be found in Ref. 7; the energy resolution of the lead glass is given by $\sigma_E/E = 0.04/\sqrt{E(\text{GeV})} + 0.015$ and the angular resolution is 0.6-0.7°. The photon-photon spectrum for photons with $E_\gamma > 200$ MeV and $E_{\gamma\gamma} > 700$ MeV is shown in Fig. 11(a). Only photon pairs in which both photons come from the same hemisphere (jet) are included. A clear π^0 signal is seen. When photons with $E_\gamma > 300$ MeV which combine to form a π^0 are removed [Fig. 11(b)] an enhancement appears at the η mass. The background subtracted spectrum is shown in Fig. 11(c) and it comprises a signal of 694 ± 93 η's. The yield of η's at the average $\sqrt{s}$ of 34 GeV was found to be $0.72 \pm 0.10 \pm 0.18$ η's per event. The η signal was divided up into three momentum bins and, following corrections for detector inefficiencies and the $\eta \rightarrow \gamma\gamma$ branching fraction, a differential η-yield was obtained. It is shown in Fig. 12. The η cross section is compared to that for $\pi^\pm$ and K^0. There is some indication in the JADE data that the η-rate might be higher in events with a planar and spherical structure than in two jet events. However, the accuracy of this measurement is not sufficient to rule out a constant η fraction for all event topologies.

TPC, $\sqrt{s}$ = 29 GeV

All $E_{\gamma\gamma}$

$1 < E_{\gamma\gamma} < 2$ GeV

452 π° entries

$2 < E_{\gamma\gamma} < 4$ GeV

610 π° entries

$4 < E_{\gamma\gamma} < 6$ GeV

103 π° entries

$\gamma\gamma$ - PAIRS/(10 MeV/c^2)

$M_{\gamma\gamma}$ (MeV/c^2)

11-83

4610A25

Fig. 8. Photon-photon invariant mass spectra as measured by the TPC.
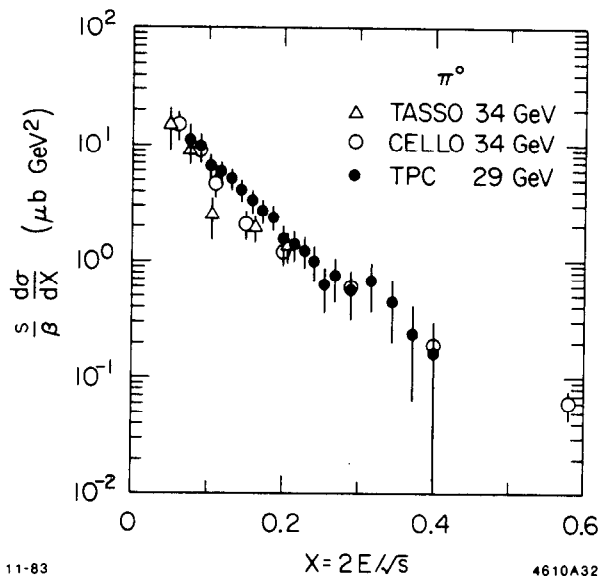
Fig. 9. Preliminary inclusive π^o cross sections from the TPC are compared with data from CELLO and TASSO.
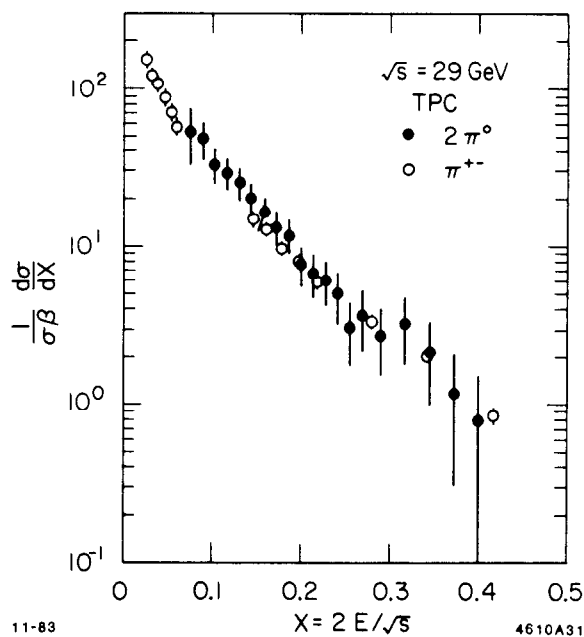
Fig. 10. Comparison of TPC π^+ and π^o inclusive cross sections.

Fig. 11. (a) Photon-photon invariant mass distribution for $E_\gamma > 200$ MeV, $E_{\gamma\gamma} > 700$ MeV from JADE. (b) Same as (a) except photons with $E > 300$ MeV which form a π^0 are removed and (c) η signal with background subtracted.

Fig. 12. JADE inclusive η-spectrum compared with $K^o, \bar{K}^o$ and $\pi^{\pm}$ from TASSO. Error bars are statistical only.

(c) Additional Measurements of Resonance Production at PEP and PETRA
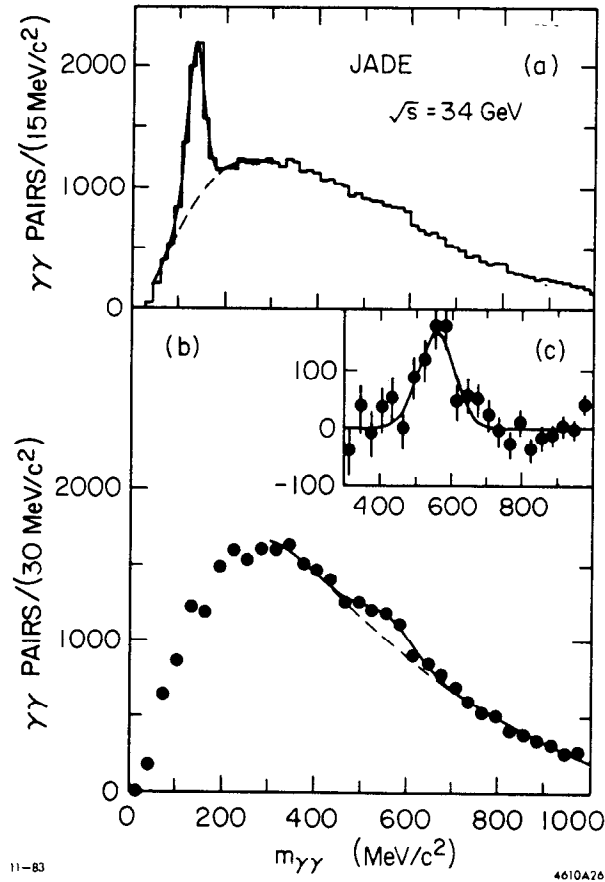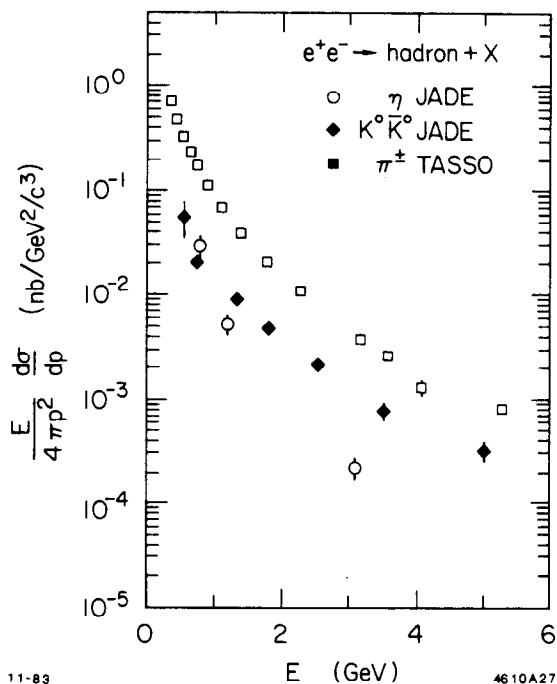
The JADE experiment has preliminary results on ρ^o and $K^{*\pm}$ production at $\sqrt{s} \approx 35$ GeV. The ρ^o is seen via the decay $\rho^o \to \pi^+\pi^-$ where both pions are required to be in the same event hemisphere. The background from random $\pi^+\pi^-$ combinations was obtained by fitting the spectrum of same sign $(\pi^{\pm}\pi^{\pm})$ combinations. Figure 13 shows the $\pi^+\pi^-$ invariant mass spectrum after this background subtraction has been made. The spectrum shows an enhancement at the ρ mass with additional contributions which are thought to come from ω and K^* reflections. These reflections have been studied with the Lund[8] Monte Carlo simulation program and a fit was performed to the spectrum in Fig. 13 which included a Breit-Wigner line shape for the ρ^o, a parametrization for the reflections whose parameters were obtained from the Monte Carlo simulation and a term for additional backgrounds. The resulting ρ^o contribution to the fit is shown in Fig. 14(a).

The $K^{*\pm}$ is seen using the decay mode $K^{*\pm} \to K_S^o \pi^{\pm}$. The $K_S^o \to \pi^+\pi^-$ decays are found using the standard procedure of forming $\pi^+\pi^-$ invariant masses for tracks whose trajectory is inconsistent with production at the event primary vertex. Mass combinations within 80 MeV/c^2 of the K_S^o mass were chosen and the π^+, π^- momenta adjusted using the known mass of the K_S^o as a constraint. The $K_S^o \pi^{\pm}$ invariant mass spectrum is shown in Fig. 15. A clear $K^{*\pm}$
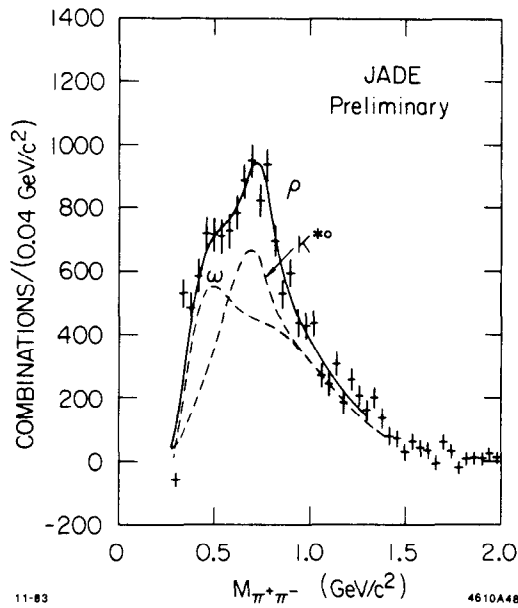
Fig. 13. Dipion invariant mass spectrum from JADE. A subtraction has been made for random $\pi\pi$ combinations. Reflections from ω and K^{*o} are indicated.
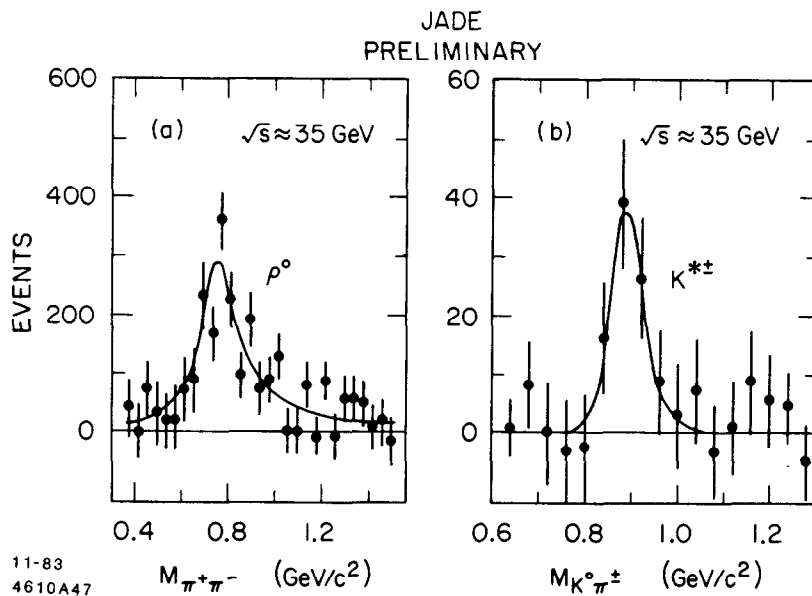

Fig. 14. JADE ρ^o (a) and $K^{*\pm}$ (b) signal after all backgrounds are subtracted.

enhancement is seen. This spectrum was fit to the sum of a Breit-Wigner line shape at a fixed K^* mass and a background term specified by four parameters. The K^* width forms the fifth free parameter. The result of the fit is shown in Fig. 15 and the background subtracted spectrum is shown in Fig. 14(b).

The LUND Monte Carlo has been used to obtain corrected particle yields and the value of r which is the parameter in the Monte Carlo which specifies the ratio of pseudoscalar (PS) mesons to vector (V) mesons. The JADE group finds $0.82 \pm 0.12 \pm 0.10$ ρ^o/event and $0.83 \pm 0.18 \pm 0.13$ $K^{*\pm}$/event. In fitting the value of r = PS/(PS + V) the parameter β, which governs the longitudinal fragmentation, was varied simultaneously with r to ensure that the charged multiplicity comes out correctly ($\langle n \rangle_{\text{charged}}$ = 13.6). The results for r are:

Fig. 15. The $K^o\pi^\mp$ invariant mass spectrum from JADE.

$$\rho^o \ : \ 0.63 \begin{array}{l} + \ 0.12 \ + \ 0.22 \\ - \ 0.11 \ - \ 0.20 \end{array}$$

$$K^{*\pm} \ : \ 0.37 \begin{array}{l} + \ 0.17 \ + \ 0.21 \\ - \ 0.15 \ - \ 0.19 \end{array}$$

$$\eta \ : \ 0.46 \begin{array}{l} + \ 0.05 \ + \ 0.10 \\ - \ 0.06 \ - \ 0.12 \end{array}$$

The observation of the η was discussed in the previous section. From spin statistics alone one would expect PS/V = 1/3 or r = 0.25. However the situation is complicated by the fact that many of the pseudoscalar particles observed arise from the decays of vector resonances. We would expect the naive spin statistics argument to hold for rank 1 particles (leading particles). Here we are averaging over all particle momenta.

The ρ^o was first studied in this energy range by the TASSO group[9] who found a yield of 0.73 ± 0.06 and a value of r = $0.42 \pm 0.08 \pm 0.15$. Hence the two experiments are in good agreement. There are no previous observations of
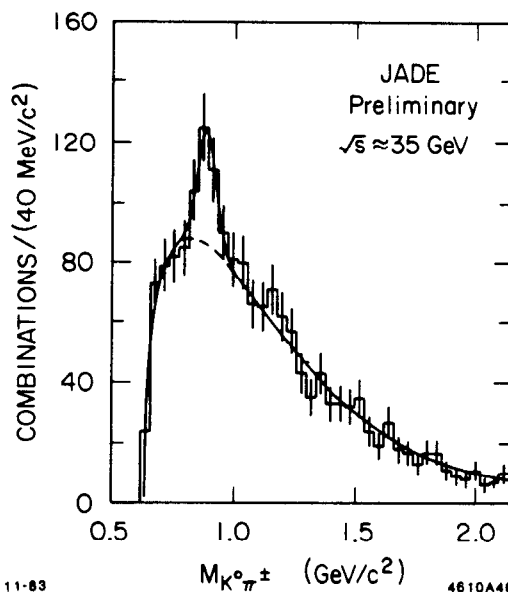
13

$K^{*\pm}$. The MARK II group has a preliminary signal of 135 ± 35 $K^{*\pm} \to K^0_S \pi^\pm$ but have yet to obtain a corrected yield or a value of r. However their signal serves as confirmation of the JADE result.

The TPC group has observed signals for both K^{*o} and ϕ. The K^{*o} is seen via its decay $K^{*o} \to K^\pm \pi^\mp$ where the $K^\pm$ and $\pi^\pm$ are positively identified using the dE/dx measurements discussed earlier. The data set corresponds to 29 pb^{-1} at $\sqrt{s} = 29$ GeV and the result is considered preliminary. Figure 16 shows the TPC $K^\pm \pi^\mp$ invariant mass spectrum. A clear signal is seen at the K^{*o}; no such signal is seen in the same sign $(K^\pm \pi^\pm)$ spectrum. The background which is shown in Fig. 16 comes from the Monte Carlo simulation. This background was parametrized with a smooth fit function and this, together with a Gaussian line shape for the K^*, was used to fit the observed spectrum. The result of this fit is shown in Fig. 16 along with the background subtracted signal which corresponds to 682 ± 82 K^{*o}. The K^{*o} efficiency as a function of momentum was obtained from the Monte Carlo simulation program; it varies from 10% at $x = 2P/\sqrt{s}$ of 0.1 to 20% at $x = 0.7$. The corrected invariant cross section is shown in Fig. 17(a) with a preliminary yield of 0.5 ± 0.1 $K^{*o} + \bar{K}^{*o}$ per event in the range $0.05 < x < 0.8$.

The TPC ϕ signal comes from reconstructing $K^+ K^-$ mass combinations where the kaons are positively identified using dE/dx. This spectrum is shown in Fig. 18. A peak is seen just above threshold which is not present in the same sign invariant mass spectrum and cannot arise from photon conversions in which the electrons are called kaons. A fit to the spectrum using a smoothed background obtained from the Monte Carlo simulation program is shown in Fig. 18 with a ϕ signal which corresponds to 53 ± 12 events. The fit yields a resonance mass of 1.02 ± 0.01 and a width consistent with the detector resolution. A preliminary ϕ inclusive spectrum is shown in Fig. 17(a) where the errors are purely statistical. For $0.05 < x < 0.4$ the ϕ yield is 0.08 ± 0.05 with no
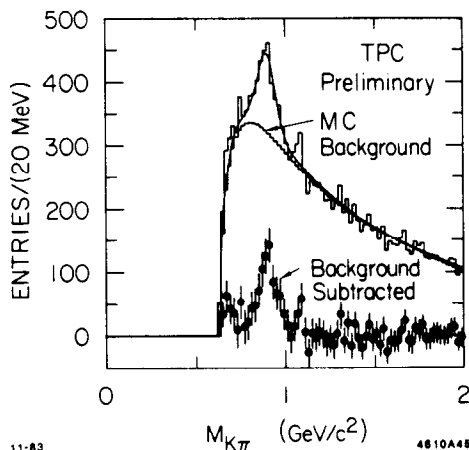

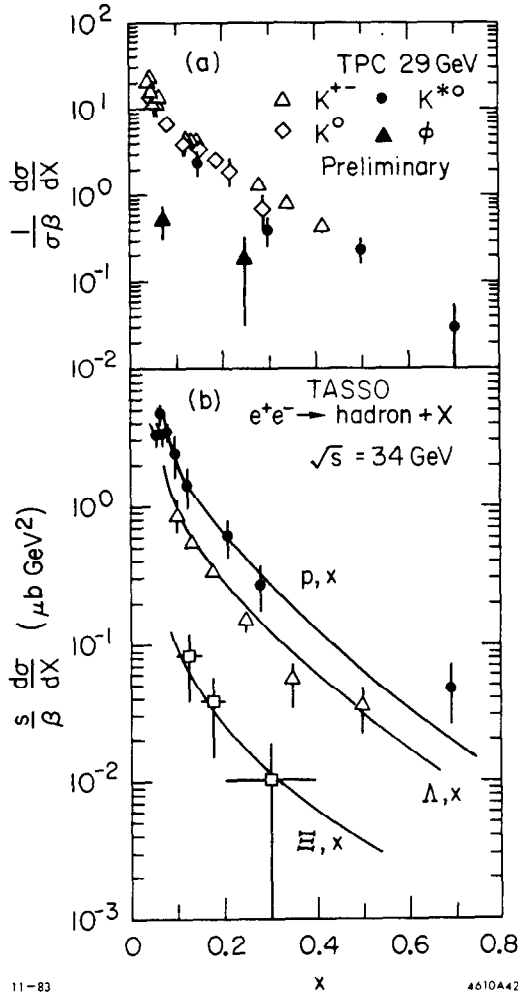Fig. 16. The $K^\pm \pi^\mp$ invariant mass spectrum from the TPC.

Fig. 17. (a) TPC inclusive spectra for $K^{\pm}$, K^o, K^{*o} and ϕ at 29 GeV. (b) TASSO inclusive spectra for Λ, p and Ξ at 34 GeV.
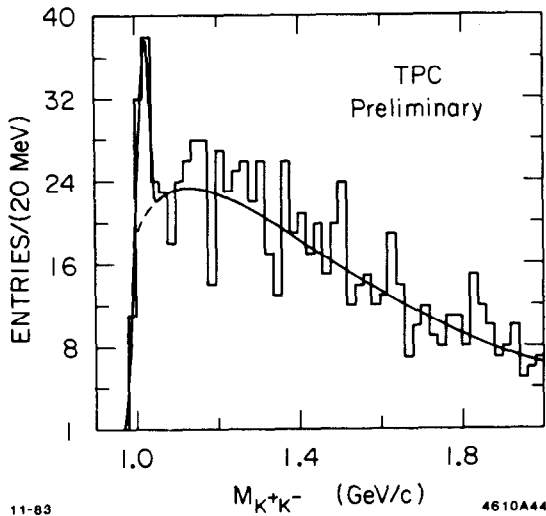

Fig. 18. The TPC K^+K^- invariant mass spectrum.

significant signal seen for $x > 0.4$. The TPC has about twice as much data in hand and with further study the ϕ production will be better understood.

The TASSO group[12] has made the first observation of Ξ^- and $\bar{\Xi}^-$ in e^+e^- annihilation. The Ξ is observed using the decay chain $\Xi^- \rightarrow \Lambda\pi^- \rightarrow p\pi^-\pi^-$. The $\Lambda \rightarrow p\pi^-$ candidates were selected by requiring that the pair momentum exceed 1 GeV/c, the p and π directions intersect in a plane transverse to the beam between 5 and 45 cm from the interaction point. The higher momentum track was assigned to the proton. The resulting $p\pi$ spectra are shown in Figs. 19(a) and (b). Λ, $\bar{\Lambda}$ candidates were chosen to have a mass within 6 MeV/c^2 of the Λ mass and these candidates were combined with an additional charged track which was assigned the identity of a pion. The crossing point of the π and Λ directions was required to have a flight path of at least 1 cm relative to the interaction point and to occur at a point closer to the interaction point than the reconstructed Λ decay point. The resulting $\Lambda\pi^-$ and $\bar{\Lambda}\pi^+$ mass spectra are shown in Fig. 19(c). A narrow peak around the Ξ mass (1.321 GeV/c^2) is visible. However no such structure is seen in the $\Lambda\pi^+$, $\bar{\Lambda}\pi^-$ spectrum, Fig. 19(d). The spectrum shown in Fig. 19 corresponds to data at average $\sqrt{s} = 14$, 22 and 34 GeV. For the sake of calculating Ξ yields and invariant cross sections, only the data at $\sqrt{s} > 30$ GeV were used. The observed events were corrected for detector inefficiencies using a Monte Carlo simulation program to yield the corrected cross section shown in Fig. 17(b). In order to account for unseen kinematic regions, the momentum spectrum was extrapolated using the shape
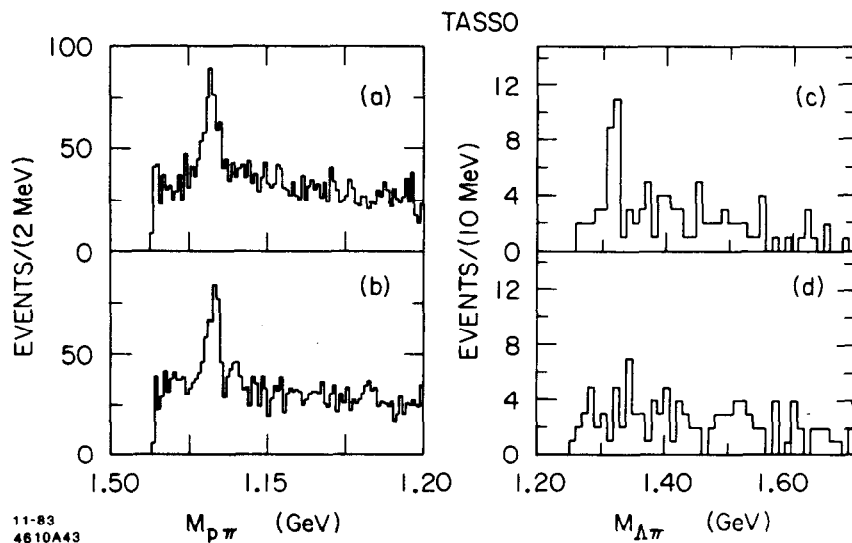

Fig. 19. Invariant mass spectra from TASSO for (a) $p\pi^-$, (b) $\bar{p}\pi^+$, (c) $\Lambda\pi^- + \bar{\Lambda}\pi^+$ and (d) $\Lambda\pi^+ + \bar{\Lambda}\pi^-$.

predicted by the LUND Monte Carlo. The fraction of the cross section resulting from this extrapolation is less than 30%. The curves in Fig. 17(b) are the predictions of the LUND model[8] with the parameter $d = 0.3$; the data are compatible with values $0.2 < d < 0.5$. The parameter d represents the suppression of the s-quark relative to the d-quark in the production of diquark pairs:

$$d = \frac{P(us)}{P(s)} \Big/ \frac{P(ud)}{P(d)} \quad .$$

At an average energy $\sqrt{s} = 34$ GeV the yield of Ξ are $0.026 \pm 0.008 \pm 0.009$ per hadronic event and the relative yields are $\Xi/\Lambda = 0.087 \pm 0.03 \pm 0.03$ and $\Xi/p = 0.033 \pm 0.011 \pm 0.011$.

It is impressive how many final state production cross sections and event yields are now measured in the e^+e^- 30 GeV energy range. This information should now be fed back into the Monte Carlo simulation programs to remove some of the flexibility which these programs have. The more we pursue these particle production measurements the better we are able to understand the 30 GeV energy region and, using data from SPEAR, DORIS and CESR, the better we are able to understand the energy dependence of the production mechanisms. We summarize in Table 1 the measured particle yields discussed here. In addition the TASSO and JADE yields are used as a constrast where measurements are not presented here. Measurements not referenced in the table are discussed for the first time here.

(d) <u>Particle Production Studies in the Υ Energy Region</u>

The CLEO[13] group has new data on the production of Λ, K^o and ϕ in the Υ energy region. The data comprise 3.5 pb^{-1} at the $\Upsilon(1S)$, 40 pb^{-1} at the $\Upsilon(4S)$ and 18 pb^{-1} in the continuum between the $\Upsilon(3S)$ and the $\Upsilon(4S)$. Hadronic events were required to have (a) a vertex consistent with the known position of the interaction point, (b) at least three charged particles emanating from the primary vertex and (c) at least 30% of the center-of-mass energy carried by the charged particles. The efficiency for the event selection is given in Table 2.

For the Λ and K^o studies "vees" were found using standard techniques which require that the vertex formed by the decay tracks be removed from the primary event vertex, that the momentum vector of the "vee" point back to the primary vertex and that the "vee" have a minimum (300 MeV/c for K^o's, 450 MeV/c for Λ's) momentum. No particle identification was used. Invariant mass spectra were generated for the decay hypotheses $K^o \rightarrow \pi^+\pi^-$ and $\Lambda \rightarrow p\pi^-$ or $\bar{\Lambda} \rightarrow \bar{p}\pi^+$. An example of the quality of the CLEO data is shown in Fig. 20. Also shown in the figure are the Monte Carlo generated efficiencies for observing Λ and K^o as a function of momentum. K^o (Λ) candidates were those for which

Table 1. Particle yields in the $\sqrt{s} = 29$-34 GeV range

Particle	Yield/Hadronic Event	Measured By
$\pi^+ + \pi^-$	10.3 ± 0.4	TASSO[1]
π^o	6.1 ± 2.0	TASSO[6]
	5.2 ± 1.8	CELLO[4]
η	$0.72 \pm 0.10 \pm 0.18$	JADE[7]
ρ^o	0.73 ± 0.06	TASSO[9]
	$0.82 \pm 0.12 \pm 0.10$	JADE
$K^+ + K^-$	2.0 ± 0.2	TASSO[1]
$K^o + \bar{K}^o$	1.6 ± 0.1	TASSO[10]
	$1.45 \pm 0.08 \pm 0.15$	JADE[11]
$K^{*+} + K^{*-}$	$0.83 \pm 0.18 \pm 0.13$	JADE
$K^{*o} + \bar{K}^{*o}$	$0.5 \pm 0.1 \quad (x < 0.8)$	TPC
ϕ	~ 0.08	TPC
$p + \bar{p}$	0.8 ± 0.1	TASSO[1]
$\Lambda + \bar{\Lambda}$	0.28 ± 0.04	TASSO[10]
$\Xi^- + \bar{\Xi}^-$	$0.026 \pm 0.008 \pm 0.009$	TASSO[12]

$|M_{\pi\pi} - M_{K^o}| < 20$ MeV/c^2 ($|M_{p\pi} - M_\Lambda| < 5$ MeV/c^2). The invariant mass spectra were fit to a smooth background and a Gaussian to establish the level of background within the selection windows discussed above. The momentum dependence of the background was obtained from mass bins adjacent to the signal bins. In addition a continuum subtraction was made for data on the resonances. An extrapolation was performed to account for unseen K^o and Λ at low momenta. This was done by fitting the corrected differential cross section and extrapolating to the unseen momentum regions. The size and uncertainty of this extrapolation is given in Table 2. Also shown in the table are other sources of systematic error — the total systematic error in the cross sections is 12%, typical relative systematic errors are $< 8\%$.

Table 2. Corrections and systematic errors (CLEO)

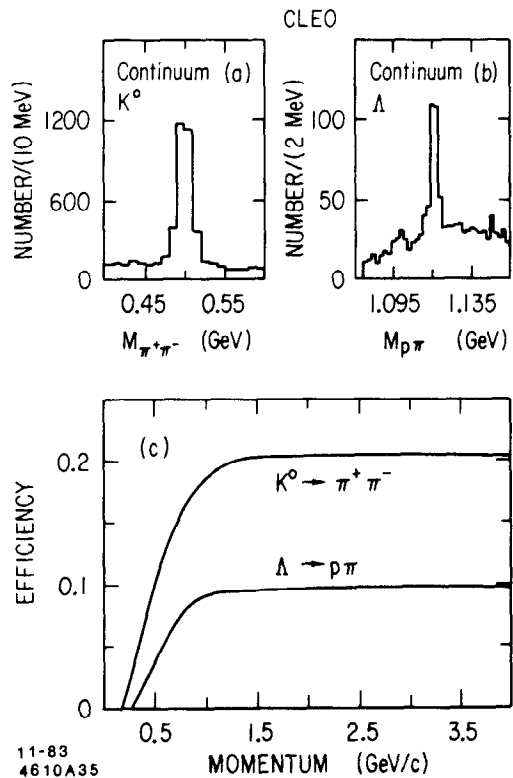| Correction	Size	Systematic Error in Cross Section
"Vee" Finding Efficiency	10% (Λ) 20% (K^o)	8%
Background Subtraction	40% (Λ) 15% (K^o)	5% (Λ) 2% (K^o)
Continuum Subtraction	60% [$\Upsilon(4S)$] 10% [$\Upsilon(1S)$]	6% 2%
Event Selection Efficiency	91% [$\Upsilon(4S)$] 88% [$\Upsilon(1S)$] 71% (continuum)	5%
Luminosity		3%
Low Momentum Extrapolation	8%	2%

Fig. 20. CLEO invariant mass spectra for (a) $\pi^+\pi^-$, (b) $p\pi$, and (c) shows the efficiency for observing $K^o \rightarrow \pi^+\pi^-$ and $\Lambda \rightarrow p\pi^-$ as a function of parent momentum.

11-83
4610A35

The number of K^o and Λ per event per GeV/c is shown in Figs. 21 and 22 respectively. The continuum spectrum is significantly harder than the $\Upsilon(1S)$. The average number of particles per event are summarized in Table 3 along with the CLEO results for charged kaons and protons submitted to this conference. Within statistics the kaon production rates in the continuum and on the $\Upsilon(1S)$ are the same and the charged and neutral rates are the same. The production of kaons increases significantly on the $\Upsilon(4S)$ presumably because of the dominance of $b \rightarrow c \rightarrow s$ in B meson decay. However for the Λ's there is a large (~ 2.5) increase in going from the continuum to the $\Upsilon(1S)$. The same increase is seen in the protons. It is interesting to speculate why the dominantly three gluon
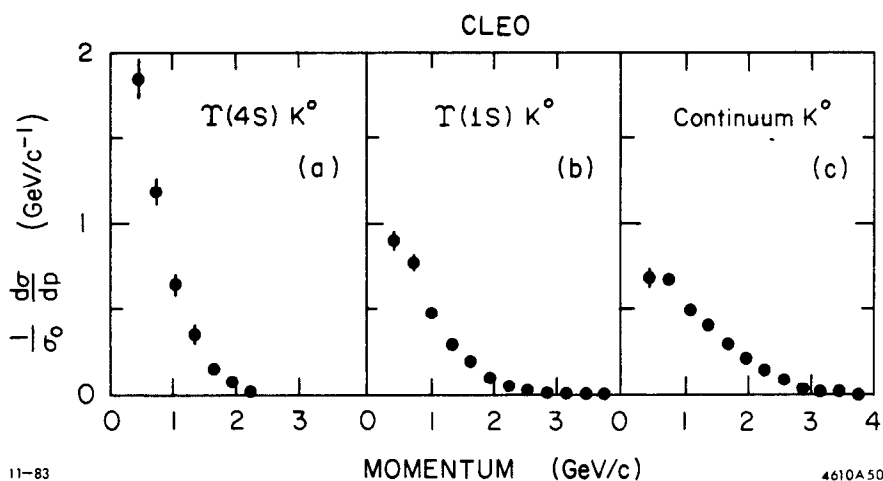

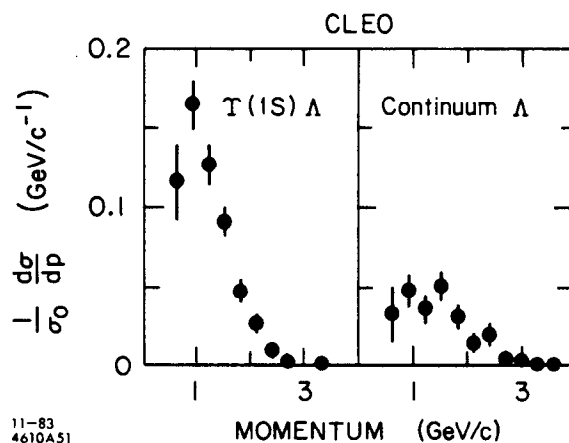Fig. 21. CLEO differential cross section versus momentum for K^o.

Fig. 22. CLEO differential cross section versus momentum for Λ.

20

Table 3. Particle yields at $\Upsilon(1S)$, $\Upsilon(4S)$ and continuum (CLEO)

	$\Lambda, \bar{\Lambda}$ / event	K^o / event	$p, \bar{p}$ / event	$K^{\pm}$ / event
continuum	0.08 ± 0.008	1.05 ± 0.025	0.114 ± 0.004	1.014 ± 0.033
$\Upsilon(1S)$	0.19 ± 0.01	0.95 ± 0.025	0.245 ± 0.005	0.991 ± 0.027
$\Upsilon(4S)$		1.46 ± 0.06		1.435 ± 0.063

final state of the $\Upsilon(1S)$ decays to baryons so much more copiously than the $q\bar{q}$ continuum state.

To study the parton fragmentation more directly, the CLEO group has plotted in Fig. 23 the inclusive cross section as a function of $z = E/E_{beam}$. For the $\Upsilon(4S)$ they assume that the spectrum results from B decays and therefore they use $z = E/(E_{beam}/2)$. It is striking how similar the cross section $s/\beta \ d\sigma/dz$ is for K^o's at the $\Upsilon(4S)$ and the continuum. This is odd since the resonance decays weakly whereas the continuum represents $q\bar{q}$ fragmentation directly. The scaling cross sections have been fit to the form Ae^{-bz} and yield the following values of b:

$$\Lambda's: \quad \Upsilon(1S) \ 13.7 \pm 0.5, \quad \text{continuum} \ 9.5 \pm 0.8$$

$$K^o's: \quad \Upsilon(1S) \ 9.9 \pm 0.2, \quad \text{continuum} \ 7.3 \pm 0.2, \quad \Upsilon(4S) \ 7.9 \pm 0.4 \ .$$
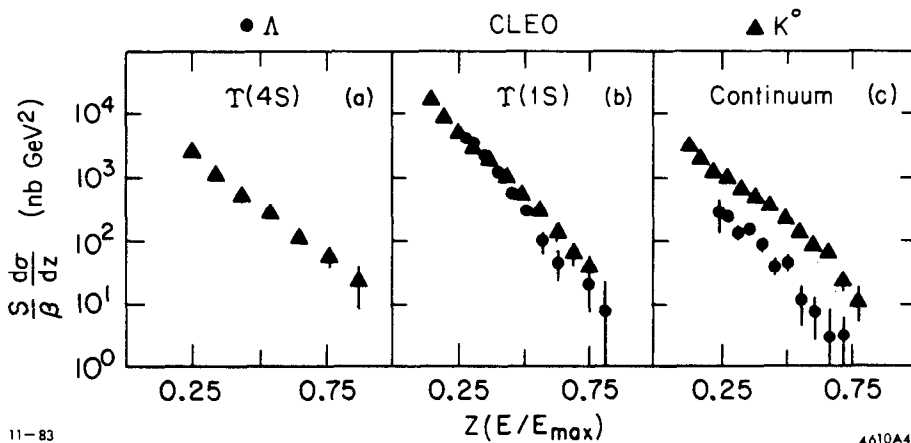

Fig. 23. CLEO inclusive spectra for K^o and Λ. Note E_{max} is equal to E_{beam} for the continuum and $\Upsilon(1S)$ but $E_{beam}/2$ for the $\Upsilon(4S)$ since each B meson carries only E_{beam}.

21

The CLEO group reconstructs ϕ's via their decay to K^+K^-. In most of the kinematic range, no positive kaon identification was required. All tracks which were not positively identified as pions by ionization or time of flight were used to form the K^+K^- invariant mass spectra shown in Figs. 24(a)-(c). For kaon momenta in the range 0.45-1.0 GeV/c positive identification was possible and hence for ϕ's in the momentum range 1-2 GeV/c a better signal to noise ratio was obtained by requiring one positively identified kaon. These invariant mass spectra are shown in Figs. 24(d)-(f). The data were fit to the sum of a smooth background and a Gaussian response function for the ϕ. This procedure was applied to three separate momentum bins to yield the number of ϕ's. This yield was then corrected for the detector inefficiencies and the unseen decay modes of the ϕ. The data on the resonances was corrected for the continuum contribution. The $\Upsilon(1S)$ data were also corrected for contributions from one photon annihilation processes to yield the ϕ meson production from direct three gluon decay. This normalized differential cross section is shown in Fig. 25 for the three gluon part of the $\Upsilon(1S)$ and the continuum. We see the same trend with the ϕ's as with the K^o's and Λ's — the continuum spectrum is harder. This is presumably no surprise and is related to the fact that the continuum shares the energy equally with two partons whereas the $\Upsilon(1S)$ decays via three partons. The yields for ϕ's per event with momenta larger than 1 GeV/c is 0.087 ± 0.012 for the continuum and 0.059 ± 0.014 for the three gluon decays of the $\Upsilon(1S)$. Extrapolating to the full momentum range using the LUND Monte Carlo yields 0.14 ϕ's per event on the $\Upsilon(1S)$ and 0.15 ϕ's per event in the continuum.

On the $\Upsilon(4S)$, the subtraction of the continuum yields a ϕ production rate of 0.00 ± 0.03 nb. If the $\Upsilon(4S)$ always decays to $B\bar{B}$, this would correspond to an upper limit (95% confidence level) for the $B \to \phi X$ inclusive branching fraction of 3% for ϕ momenta above 600 MeV/c.

(e) Tagged D$^\pm$, D^o and D*; the Charm Fragmentation Function

New data on D^* production are now available from the HRS, DELCO and CLEO and on direct D production from the HRS and CLEO. The D^* is studied via its decay $D^{*\pm} \to D^o \pi^\pm$. The DELCO group observes the D^o in its decay mode $K\pi$, $K3\pi$ and $K\pi X$ where their mass window of the D^o is sufficiently wide to include the latter decay even though the third decay product (X) is not seen. The DELCO experiment uses data comprising 90 pb^{-1}. The analysis proceeds by two methods: (a) either the π or K from the D^o decay is positively identified using their Cerenkov counter or (b) time of flight is used to positively identify the kaon. These selections favor high momentum and low momentum D^*'s respectively. Because of the positive identification of the D^o decay product, DELCO is able to measure their background using events for which the
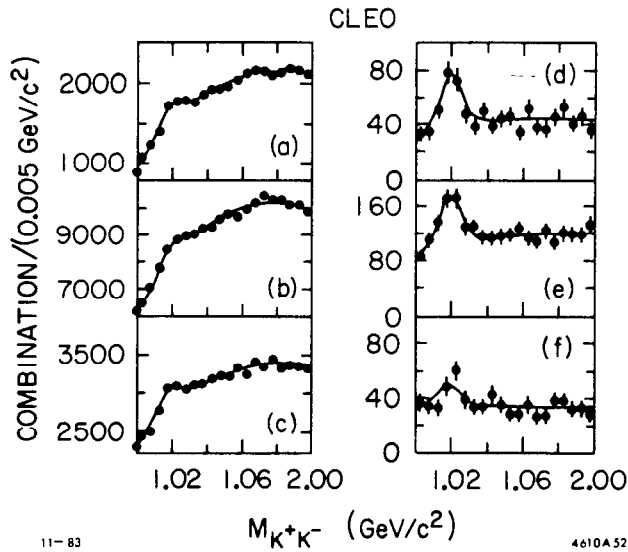
Fig. 24. CLEO K^+K^- invariant mass spectra for $\Upsilon(1S)$ (a) and (d), $\Upsilon(4S)$ (b) and (e) and continuum (c) and (f). No particle identification is used in (a)-(c); one identified kaon is required for (d)-(f).
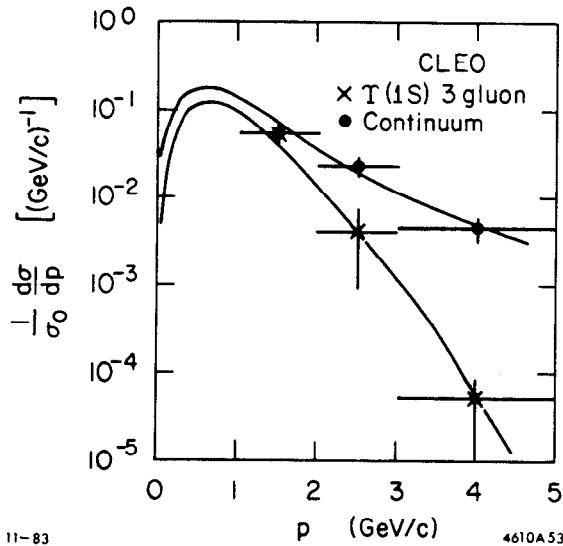
Fig. 25. The CLEO differential cross section versus momentum for ϕ's.

bachelor π in the $D^{*\pm}$ decay has the wrong sign relative to the kaon in the D^o decay. The mass difference, Δ, between the reconstructed $D^o\pi^+$ and the D^o is shown for the DELCO data in Fig. 26.
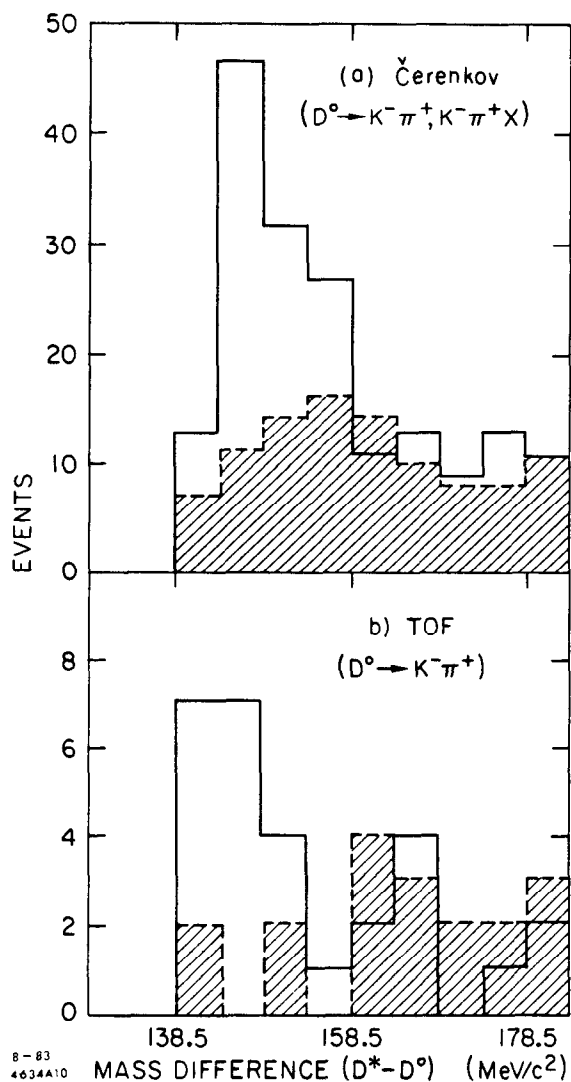
Fig. 26. The mass difference $\Delta = M(D^o\pi^+) - M(D^o)$ is shown for the DELCO experiment. (a) Using the Cherenkov tag and (b) using the time of flight tag. The shaded region is an estimate of the background obtained from wrong sign K's.

The power of excellent momentum resolution shows up strikingly in the HRS data. They have two data sets, one comprising 19.6 pb^{-1} and another, whose results are preliminary, which comprises 80 pb^{-1}. Results from both are presented here. The HRS observes the $D^* \to D^o\pi^+$, $D^o \to K^-\pi^+$ decay chain where no particle identification is used. Figure 27 shows their plot of Δ for the 80 pb^{-1} data set. Four regions of $z = 2E_{D^*}/\sqrt{s}$ are shown — there is good evidence for a signal at $z < 0.4$. The HRS also has a clear signal in their 19.6 pb^{-1} data set.

Fig. 27. Δ from HRS with $1.81 < M(K\pi) < 1.92$ GeV/c^2 for the z intervals shown.

The measured cross sections $\sigma(D^{*+} + D^{*-})$ are $0.15 \pm 0.02 \pm 0.04$ nb ($z >$ 0.35) for DELCO and 0.10 ± 0.04 nb (19.6 pb^{-1} data set) and 0.11 ± 0.04 nb (80 pb^{-1} data set) for the HRS. These can be contrasted to the MARK II[14] result of 0.25 ± 0.13 nb at $\sqrt{s} = 29$ GeV and TASSO[15] of $0.09 \pm 0.02 \pm 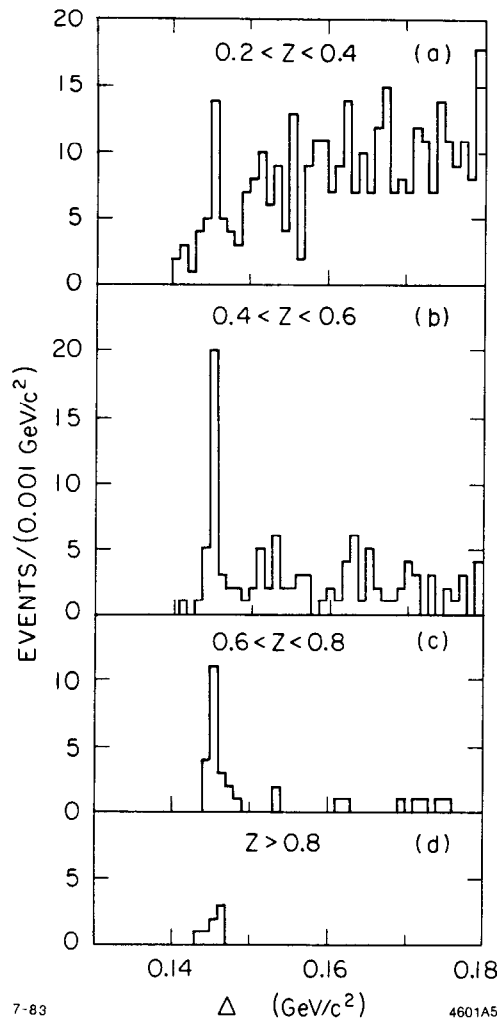0.03$ ($z > 0.3$) at an average $\sqrt{s} = 34.4$ GeV. The corrected inclusive cross section $s/\beta \, d\sigma/dz$ is shown in Fig. 28 for the four experiments which have made measurements in this energy region. The trend of the charm fragmentation function shown in Fig. 28 is that charm is "hard" — the $\langle z_{D^*} \rangle$ is found to be 0.56 ± 0.02 (HRS), $0.57 \pm 0.02 \pm 0.05$ (DELCO) and 0.59 ± 0.06 (MARK II). The fragmentation function has been fit to the form suggested by Peterson et al.[16]

$$D_Q(z) = \frac{A}{z\left(1 - \frac{1}{z} - \frac{\epsilon_Q}{1-z}\right)^2} \tag{1}$$

where Q denotes a heavy flavor species and $\epsilon_Q \approx M_Q^{-2}$. The values found for ϵ_c are 0.36 ± 0.12 (19.6 pb^{-1}) and 0.29 ± 0.11 by HRS, 0.79 by DELCO, 0.18 ± 0.07 by TASSO and 0.14 ± 0.03 by CLEO (see later in this section). There are two
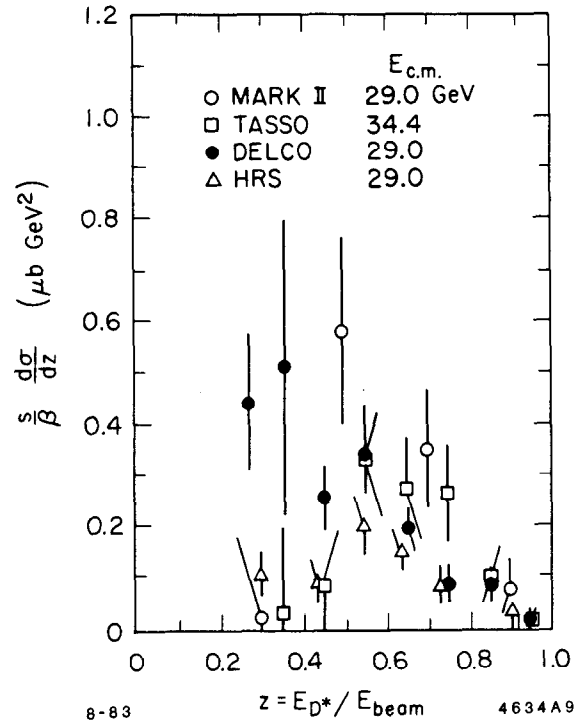

Fig. 28. The $D^{*\pm}$ inclusive cross sections for all experiments at PEP and PETRA.

comments in order here: (a) the shape of $D_Q(z)$ varies slowly with ϵ_Q and the large variation in ϵ_Q above does not represent a major difference in shape and (b) the fits have been made directly to the observed $s(d\sigma/dz)$ spectra. Radiative effects tend to lower the effective $\sqrt{s}$ and hence raise the measured value of z. This has not been taken into account in the above determinations.

One can conclude from these studies that considerably more data are needed before the charm fragmentation function is well understood. By the same token more data are needed to pin down accurately the charm cross section in the 30 GeV energy region.

The CLEO group[17] has studied the production of D^*'s in the Υ energy region. The total data sample consists of 150,000 resonant hadronic events which corresponds to an integrated luminosity of 60 pb^{-1} at an average $\sqrt{s} =$ 10.5 GeV. The D^*'s are found in the usual manner (same as HRS discussed earlier). Requiring $|\Delta - 145.4| < 1.5$ MeV/c^2 provides a signal of 268 ± 41 D^*'s — the $K^+\pi^-$ invariant mass for these D^* candidates with momenta above 3 GeV/c is shown in Fig. 29. CLEO measures an inclusive cross section[18] for $D^{*\pm}$ of $0.87 \pm 0.10 \pm 0.28$ nb for $x > 0.35$ where $x = p/p_{max}$ (CLEO chooses the variable x because then all experiments have the same kinematic range: if

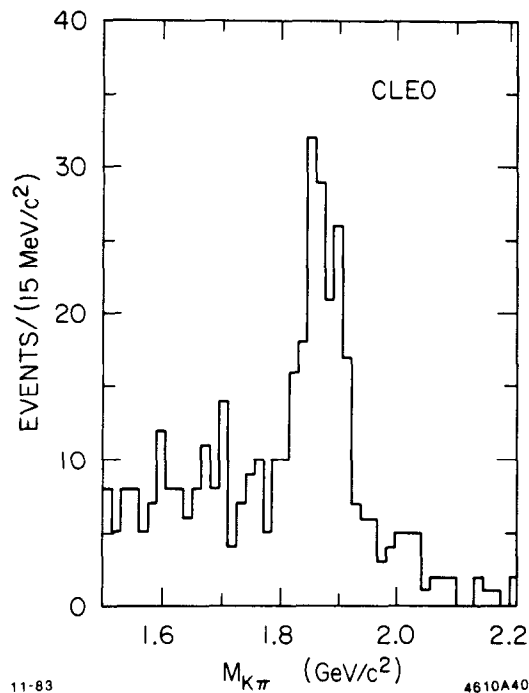Fig. 29. The CLEO $K^+\pi^-$ invariant mass spectrum where $143.9 < \Delta < 146.9$ MeV/c^2 was required and $P_{K\pi\pi} > 3$ GeV/c.

scaling holds x is as useful a variable as z). The corrected cross section $s(d\sigma/dx)$ is shown in Fig. 30(a) along with the data of MARK II and TASSO. The fit shown as a solid line is to (1) above with the scaling variable x ($\epsilon_x = 0.10 \pm 0.02$) and as a dashed line using the scaling variable z ($\epsilon_z = 0.14 \pm 0.03$). Assuming that there are an equal number of charged and neutral D^*'s produced and that the charm cross section is 40% of the total hadronic cross section, CLEO estimates that $65 \pm 7 \pm 21\%$ of charmed quarks produced fragment into D^*'s with $x >$ 0.35.

CLEO is also able to see the direct production of D^o via the decay $D^o \rightarrow K^-\pi^+$. $K\pi$ invariant mass combinations were formed for all oppositely charged particle pairs for which $|\cos\theta_K| < 0.75$, where θ_K is the decay angle of the K in the $K\pi$ rest frame. This cut does not severely limit the D^o efficiency since the D^o has spin zero. However it strongly disfavors the background which is peaked at $|\cos\theta_K| = 1$. The invariant mass spectrum for $P_{K\pi} > 2.5$ GeV/c is shown in Fig. 31. The D^o signal comprises 644 ± 80 events and corresponds to a corrected inclusive cross section of $1.6 \pm 0.3 \pm 0.3$ nb for D^o with $x > 0.3$. The differential D^o production cross section is shown in Fig. 30(b) along with the MARK II data.
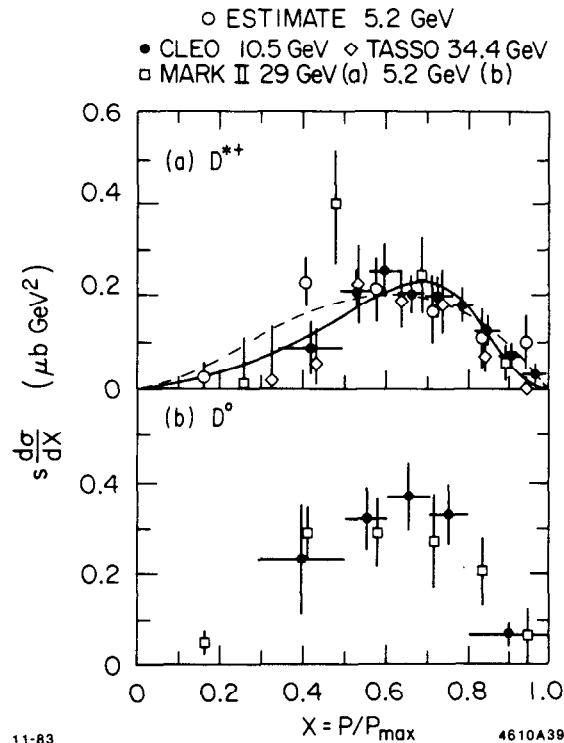

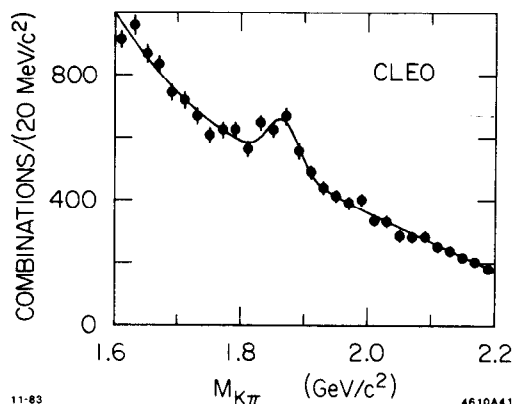Fig. 30. The inclusive cross section as a function of x is shown for $D^{*\pm}$ in (a) and D^o in (b).

Fig. 31. The CLEO $K^-\pi^+$ invariant mass spectrum is shown for $P_{K\pi} > 2.5$ GeV/c and $|\cos\theta_K| < 0.75$.

The CLEO group is able to use their D^* and D^o data to estimate how often a D^o is produced directly. Since the D^o is observed in both analyses in the same decay mode, the uncertainty in this D^o branching fraction drops out. Assuming all D^*'s decay to D^o and that D^{*o} production is equal to D^{*+} production, CLEO obtains a cross section for direct D^o production of $0.12 \pm 0.15 \pm 0.14$ nb for $x >$ 0.55. This corresponds to a D^o/D^{*+} production ratio of $0.18 \pm 0.24 \pm 0.25$ for $x > 0.55$. This result is consistent with both 0 and 1/3, the result from naive spin statistics. It seems unlikely that they are produced equally at this energy.

The HRS experiment is able to exploit their excellent momentum resolution to observe D^o and D^+ directly at PEP. Figure 32 shows the $K^{\pm}\pi^{\mp}$ and $K^{\pm}\pi^{\mp}\pi^{\mp}$ invariant mass distributions for the indicated z cuts. The distributions are from their 19.6 pb^{-1} data set. The fits shown in Fig. 32 are used to extract the following ratios: $D^o/D^{*+} = 1.7 \pm 0.7$ $(z > 0.4)$, $D^o/D^+ = 2.3 \pm 1.2$ $(z >$ 0.5). If we assume that D^{*o} always decays to D^o and that $B(D^{*+} \to D^o\pi^+) =$ 0.44 then, if all D^o came from D^*, the ratio D^o/D^{*+} would be 0.7. The HRS data indicate then that at $\sqrt{s} = 29$ GeV there could be significant direct D^o production.

(f) High P$_t$ Leptons As a Tag for b and c Quarks; the b and c Quark Fragmentation Functions

The MARK II experiment was the first experiment to use high P_t electrons as a means of tagging b and c quark decays[19] and thereby obtaining the first indication of the b quark fragmentation function. Since then results have followed from the MAC group (muons),[20] the MARK J group[21] (muons) and the TASSO group (electrons). The MARK II has updated its electron analysis and
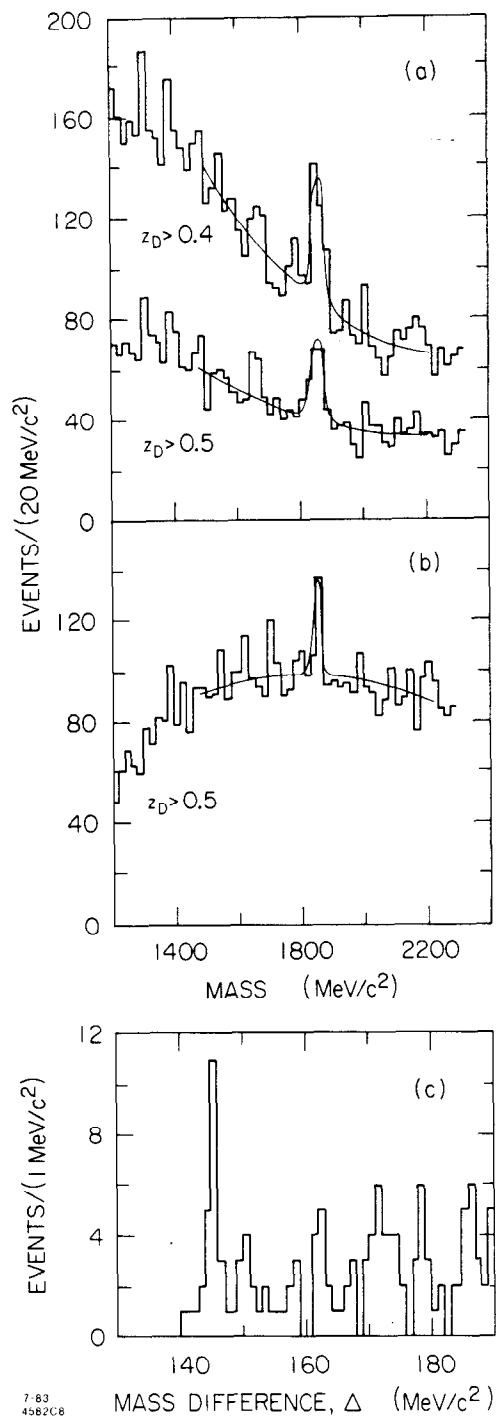
Fig. 32. HRS data for (a) $K\pi$ invariant mass for $Z_D > 0.4$ and $Z_D > 0.5$ and (b) $K\pi\pi$ invariant mass distribution for $Z_D > 0.5$. Shown in (c) is the plot of Δ for the same 19.6 pb^{-1} data set.

completed its muon analysis. Since three of the four analyses are published and the fourth (TASSO) follows the same basic analysis pattern, we present here a general outline of the analysis procedure and focus rather on the results. Leptons are identified in hadronic events and their momentum transverse to the thrust axis (P_t) is measured. The data are then divided into bins of P and P_t. Background sources are calculated and/or measured and a fit is done to the data in which one permits as sources for the leptons semi-leptonic decays of bottom quarks, charm quarks and background. As an example typically a b-enriched sample (large P, large P_t) will comprise leptons which are 60% from b, 20% from c and 20% background. The fits require input from the Monte Carlo simulation programs which will specify the efficiency for a given P and P_t bin as a function of the parameters which specify quark fragmentation functions. The semileptonic branching fractions are also parameters in the fits. As an example of the quality of the data, Fig. 33 shows the TASSO electron yields $(P > 2$ GeV/c) as a function of P_t where the backgrounds have been subtracted. Figure 34 displays the same information from the MARK J in terms of a normalized cross section versus P_t^2. All experiments use the parametrization given in (1) for the fragmentation function. However the MARK J quote results for $\sqrt{\epsilon_Q}$ not ϵ_Q. The results of the fits to the data are summarized in Table 4(a) for b quarks and 4(b) for c quarks. The agreement between the experiments for $\langle z \rangle_b$ is most striking — b quark fragmentation is very hard with the primary B meson taking typically 75-80% of the available quark energy. As an example of what the parameters in Table 4 mean, Fig. 35 shows the fragmentation function obtained from the MARK J fit for charm (a) and bottom (b) quarks. The dashed lines represent the 1σ errors for the fits.
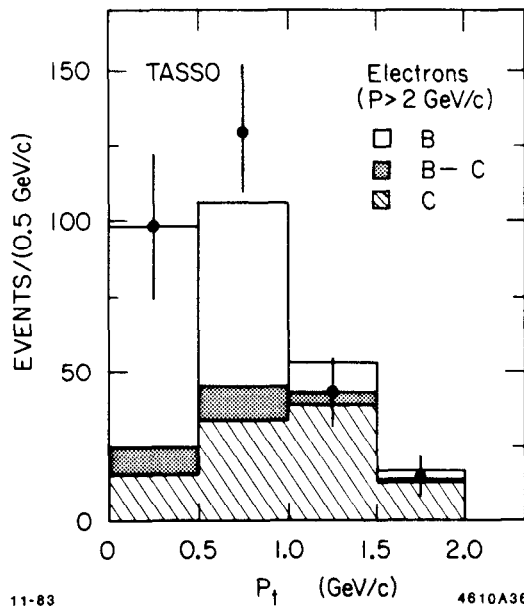
Fig. 33. TASSO electron yields as a function of P_t for $P > 2$ GeV/c. The fitted source for the lepton is indicated and background contributions are subtracted.
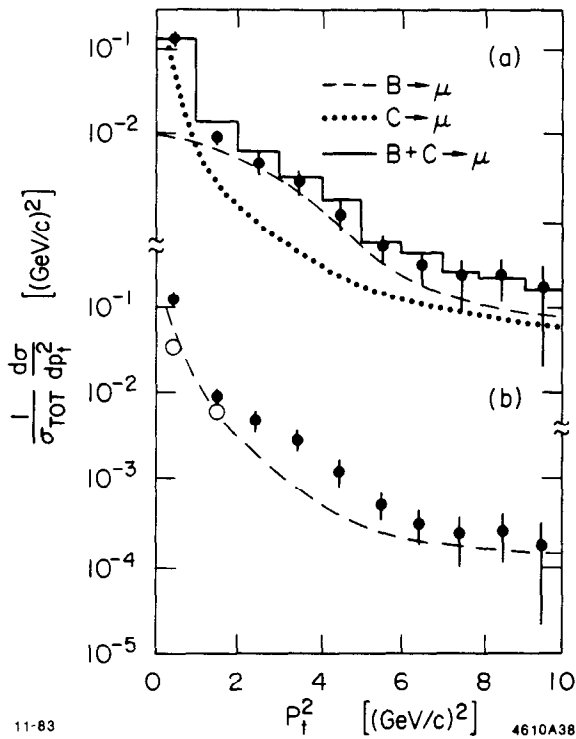
Fig. 34. The MARK J data are shown as a function of P_t^2. (a) The data are compared to the Monte Carlo predictions for the muon parents shown and (b) the cross section is shown for $P > 2$ GeV/c by the open circles and for all momenta for the solid circles. The two spectra differ only for $P_t^2 < 2.0$ (GeV/c)^2.
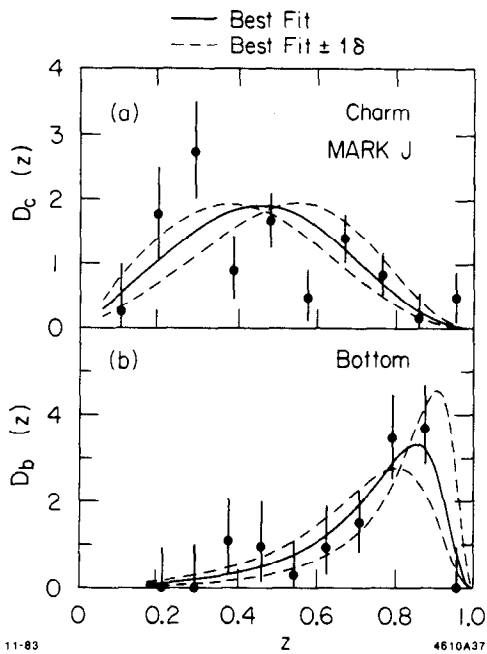
Fig. 35. Data and fit results from the MARK J for the charm (a) and bottom (b) fragmentation functions.

Table 4. b and c quark fragmentation parameters

(a) Bottom Quarks

	ϵ_b	$\langle z \rangle_b$
MARK II (e)	$0.015 {\,+\,0.022 \atop \,-\,0.011} {\,+\,0.023 \atop \,+\,0.011}$	$0.79 \pm 0.06 \pm 0.06$
(μ)	$0.042 {\,+\,0.218 \atop \,-\,0.041} {\,+\,0.12 \atop \,+\,0.035}$	$0.73 \pm 0.15 \pm 0.10$
MARK J (μ)	$0.15 \pm 0.03 \pm 0.05^*$	$0.75 \pm 0.03 \pm 0.06$
MAC (μ)	$0.008 {\,+\,0.037 \atop \,-\,0.008}$	0.80 ± 0.10
TASSO (e)	$0.022 {\,+\,0.037 \atop \,-\,0.016} {\,+\,0.020 \atop \,+\,0.012}$	0.75 ± 0.08

(b) Charm Quarks

	ϵ_c	$\langle z \rangle_c$
MARK J (μ)	$0.8 \pm 0.1 \pm 0.2^*$	$0.46 \pm 0.02 \pm 0.05$
TASSO (e)	$0.23 {\,+\,0.35 \atop \,-\,0.16} {\,+\,0.17 \atop \,+\,0.08}$	$0.55 {\,+\,0.11 \atop \,-\,0.09}$

* MARK J measures $\sqrt{\epsilon}$.

3. QCD TESTS IN e^+e^- IN THE 30 GeV ENERGY REGION

In this section we consider new data from PEP and PETRA in the area of QCD tests.[22] During the last year the experimental groups have begun to do $O(\alpha^2)$ QCD tests and there is general agreement that α_s obtained in this way is reduced by about 20%. We will look into the evidence for differences in quark and gluon fragmentation and data pertaining to correlations between forward and backward jets.

(a) <u>Measurement of α_s</u>

Three approaches to the measurement of α_s are presented here

(i) The measurement of R (JADE).

(ii) Energy-energy correlations (MARK J, CELLO and MAC).

(iii) Shape analyses (TASSO).

The JADE group has made a study of R, the ratio of the hadronic cross section to the mu-pair cross section, as a function of $\sqrt{s}$. The advantage of this approach

is that QCD has a "gold plated" prediction namely

$$R = 3 \sum_q e_q^2 \left\{ 1 + \frac{\alpha_s}{\pi} + C_2 \left(\frac{\alpha_s}{\pi}\right)^2 \right\} \qquad (2)$$

and terms of higher order in α_s/π can be safely ignored. In Eq. (2) above q is an index for quark flavor and ranges over those quark pairs which are above the threshold. e_q is the quark charge and in the $\overline{MS}$ scheme $C_2 = 1.99 - 0.12 \, N_f$, where N_f is the number of flavors. The JADE data for R as a function of $\sqrt{s}$ is shown in Fig. 36 and yields $\langle R \rangle = 3.97 \pm 0.05 \pm 0.10$. These data are fit to the sum of Eq. (2) and a contribution from the weak propagator (Z^o) to yield

$$\sin^2 \theta_W = 0.23 \pm 0.05 \qquad \text{and} \qquad \alpha_s = 0.20 \pm 0.08 \quad .$$

Unfortunately this "gold plated" test of α_s yields an experimental result of limited accuracy.

Before we can discuss the tests listed under (ii) and (iii) we are forced to digress for a moment to discuss Monte Carlo models. All the subsequent tests discussed in this section will rely on corrections which are made using models — models both for the QCD matrix elements and for the fragmentation of the quarks and gluons whose dynamics is specified by the matrix elements. The main distinguishing element in the implementation of QCD itself is the use of models for the inclusion of second order effects. There are two main classes of models[23] which are widely used in $e^+ e^-$ physics — the string approach embodied in the LUND Monte Carlo[8] and the independent jet models, examples of which are the Ali et al.,[24] and the Hoyer et al. model.[25] For convenience we will refer to these
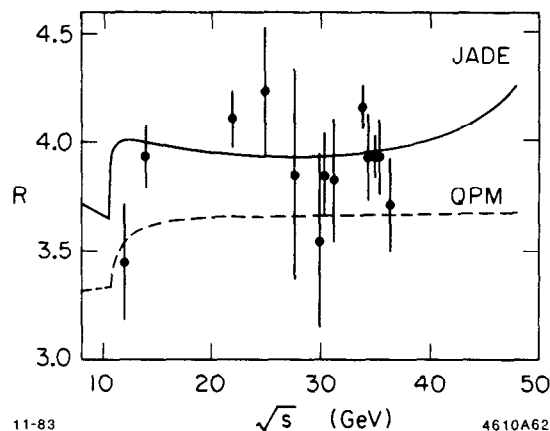

Fig. 36. R as a function of $\sqrt{s}$ from JADE.

two different approaches as STR and IF. We consider first the perturbative input to the models. For two jet topologies there is no difference in the models, but for the three jet (and four jet) topologies the models are different as illustrated in Fig. 37. Figure 37 shows the production of a $q \bar{q} g$ parton state in the limit where there are no transverse degrees of freedom ($\sigma_q = 0$) in the hadronization. In Fig. 37(b) (IF) the three partons will fragment independently of each other, the hadrons will be produced along the direction of the partons and the probability of a particular parton kinematic configuration is specified by the QCD matrix elements. In Fig. 37(a) the q and $\bar{q}$ are formed by a string — the $q \bar{q} g$ final state arises when the string is plucked transversely. The string will eventually break as a $q' \bar{q}'$ pair are pulled from the vacuum. The LUND model then decays the $q \bar{q}'$, $q' \bar{q}$ systems in their own rest frames and transforms the hadrons back into the laboratory frame. So even if $\sigma_q = 0$ in the decay of each $q \bar{q}$ system, the hadrons in the laboratory frame do not all follow the parton directions. In the LUND model the color strings have coupled the jets. Until recently, these models employed either first order QCD diagrams only or the second order diagrams shown in Fig. 38(a). More recently people have been incorporating the virtual diagrams shown in Fig. 38(b). However there are two different theoretical approaches to the calculation of the virtual diagrams. The first approach, commonly referred to as the ERT or VGO scheme, is due to two groups; Ellis, Ross and Terrano[26] and Vermasseren, Gaemers and Oldham[26] while the second, so called FKSS scheme, is due to Fabricius, Kramer, Schierholtz and Schmidtt.[27] There was an apparent disagreement in the size of the virtual corrections as calculated by ERT (VGO) and FKSS. However this has now been resolved (see for instance, Ref. 28) as a difference in the way the "cutoffs" have been applied. The cutoff parameters are used to decide when a final state is 3 versus 4 partons, 2 versus 3 partons etc. There are two basic schemes used for cutoffs: (a) the definition of a jet in terms of the Sterman-Weinberg[29] variables ϵ, δ and (b) the use of the variable $y_{ij} = M_{ij}^2 / \sqrt{s}$ where i and j refer to two partons with mass M_{ij}. If y_{ij} is less than y_0 the two partons are recombined into one. Typical values used in analyses are $y_0 \sim 0.02$, $\epsilon_0 \sim 0.1$ and $\delta \sim 15^o$.
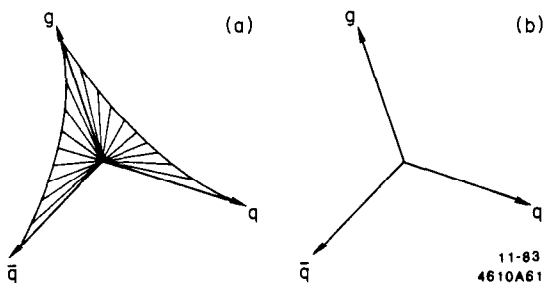
Fig. 37. Artist's perception of the difference between qqg decay in the string picture (a) and the independent fragmentation picture (b). For these pictures $\sigma_q = 0$.
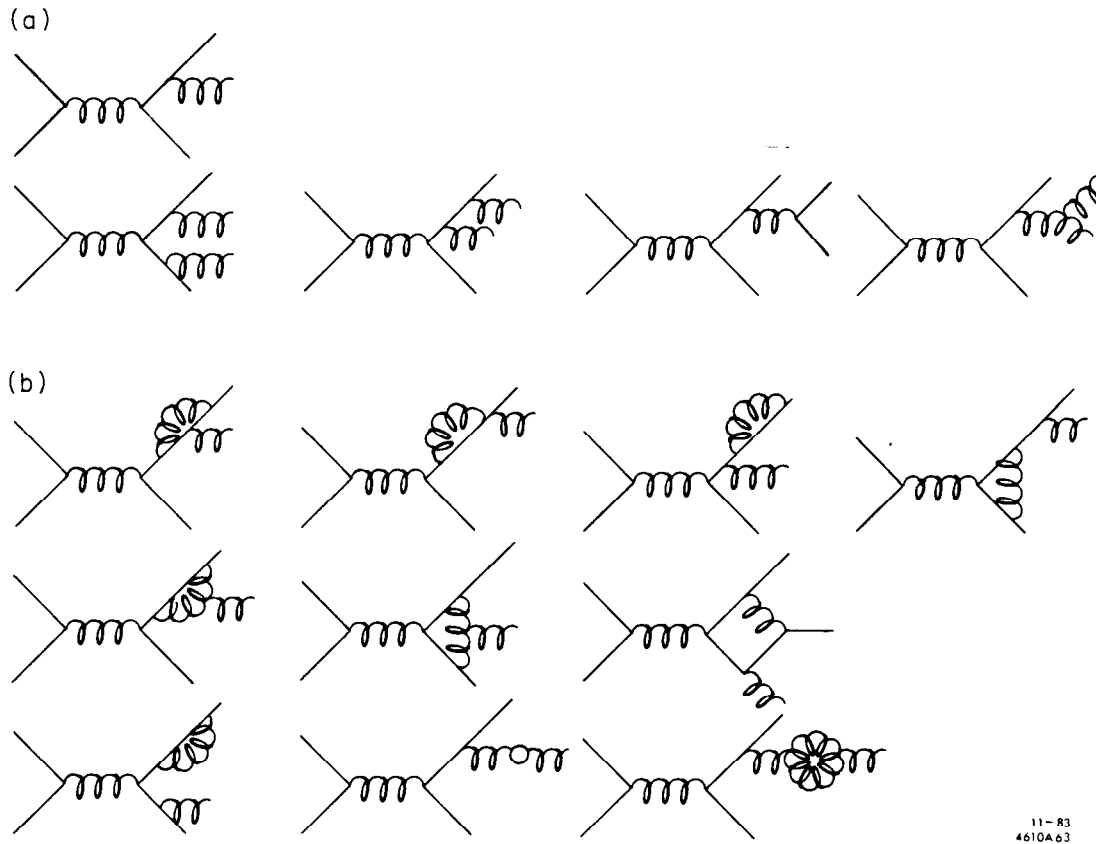
Fig. 38. (a) Tree level diagrams for 3 and 4 parton final states and (b) second order virtual parton contributions.

We see that the two classes of models for the perturbative QCD differ in their approach to the problem and it would be very surprising if their predictions for e^+e^- hadronic events were identical. We would like to stress here that in a sense these two models form two different <u>extremes</u> and that the real world probably lies somewhere in between. Why do they form two extremes? As long as Λ extracted using the LUND approach is coming out 500-1000 MeV, the color string must be stretching very far before it breaks. This is extreme because it would seem energetically more favorable to break the string earlier and pull a $q\bar{q}$ pair from the vacuum. At the other extreme however the IF models ignore color correlations completely. As an additional shortcoming, neither model incorporates the effects of soft gluons which could be important at these energies ($\approx$ 30 GeV). Finally, the implementation of the virtual diagrams provides another possible "knob" in the Monte Carlo program and everybody's "knobs" are not set to the same position.

More "knobs" are introduced in the nonperturbative (hadronization) inputs of the models. The LUND model has either standard Feynman-Field[30] fragmentation or its own fragmentation model. The IF models use the Feynman-Field approach. They are many inputs into these fragmentation models — parameters which govern the transverse and longitudinal fragmentation of quarks and gluons, the pseudoscalar to vector fraction for primary mesons, the relative probability to produce a $u\bar{u}$, $s\bar{s}$ and $d\bar{d}$ quark pair from the vacuum, the diquark probability, branching fractions etc.

The message is then clear — as long as tests of QCD rely on models it is hard to compare two different analyses because the Monte Carlo simulations can differ in many ways. It is no longer reasonable to assume that one group's "LUND" is equivalent to another group's "LUND" — they can differ in the implementation of the virtual diagrams, the fragmentation parameters, the choice of fragmentation model, etc. This is an unfortunate situation and experimental groups, in cooperation with the authors of the simulation programs, should try to allot some time to making the models more uniform.

Table 5 summarizes measurements of α_s, with corrections to $O(\alpha_s^2)$, using the two different approaches to the implementation of QCD. The JADE result has been available for quite some time;[32] the other three results are more recent. Before we discuss the measurements it is worth observing that while the experiments differ in degree, they are all consistent with the trend that $\alpha_s(\text{STR})$ > $\alpha_s(\text{IF})$ namely that α_s obtained using the LUND model is larger than α_s obtained using the IF models. In the light of the previous discussions this should not come as a surprise, since one expects naively to have more three jet events in the LUND approach than in the IF approach. Before drawing more conclusions we will look at the data.

Table 5. Comparison of α_s Results to $O(\alpha^2)$

Experiment	α_s (IF)	α_s (STR)	Method
MARK J[31]	0.12 ± 0.01	0.14 ± 0.01	Energy-Energy Correlations
CELLO	0.12 ± 0.02	0.19 ± 0.02	Energy-Enegy Correlations
TASSO	0.16 ± 0.02	0.21 ± 0.02	Combined Fit to Many Distributions
JADE[32]	$0.16 \pm 0.015 \pm 0.03$	$0.16 \pm 0.015 \pm 0.03$	Fit to X_1, $X_\perp$

The MARK J[31], CELLO and MAC experiments have used the energy-energy correlation to measure α_s. The energy-energy correlation[33] involves using hadronic events to study the energy weighted cross section

$$\frac{1}{\sigma}\frac{d\Sigma}{d\cos\chi} = \frac{1}{N}\sum_N \sum_{i,j} \frac{E_i E_j}{E_{vis}^2} \Delta(\cos\chi_{ij})$$

where the sum ranges over all N events including all particle pairs i and j with energies E_i and E_j. The particles i and j are separated by the angle χ_{ij}. Two jet events will give rise to peaks at $\cos\chi = \pm 1.0$ in the absence of any transverse momentum in the fragmentation. The presence of this hadron P_t will provide correlations at other values of $\cos\chi$. Gluon emission will provide an asymmetry to the energy correlation. Hence to isolate such an emission one studies the asymmetry

$$A(\cos\chi) = \frac{1}{\sigma}\left\{\frac{d\Sigma}{d\cos\chi}(\pi-\chi) - \frac{d\Sigma}{d\cos\chi}(\chi)\right\} \quad . \tag{3}$$

If all sources of nonperturbative effects were symmetric, one could hope to project out the perturbative QCD using Eq. (3). So the hopes were that the energy correlation would

(a) minimize the effects of fragmentation;

(b) reduce the soft hadron. effects via the use of the energy weighted correlation;

(c) permit therefore a direct comparison between the data and the perturbative QCD calculations, i.e. reduce to a minimum the use of models in the determination of α_s.

A little history is now in order. In 1980 PLUTO[34] showed that $1/\sigma\, d\Sigma/d\cos\chi$ was fragmentation dependent and hence one should use the asymmetry $A(\cos\chi)$. In 1982 the MARK II group[35] showed that the fragmentation of the $q\bar{q}g$ state contributes an asymmetry about 20% of the predicted perturbative effect. Since this contribution from fragmentation is a nonperturbative effect, comparison between data and perturbative QCD would lead to an incorrect determination of α_s. In 1982 the CELLO group[36] concluded that $A(\cos\chi)$ was influenced by nonperturbative fragmentation. In 1982 Steve Ellis[37] used the string picture to confirm the result of the MARK II. In 1982 Ali and Barreiro[38] put in second order QCD and showed that it had a small effect on $A(\cos\chi)$ but reaffirmed that the fragmentation of the $q\bar{q}g$ parton state contributed about a $\sim 20\%$ component to $A(\cos\chi)$, and that this effect persisted at all values of $\cos\chi$. The result of this history lesson then is that it is very hard to compare perturbative

QCD calculations directly with the data. Unhappily this returned the energy correlation measurement back to the uncertain land of the Monte Carlo models.

The MARK J group[31] have used the Ali et al. Monte Carlo with Feynman-Field fragementation as their IF model and the LUND model with Feynman-Field fragmentation as their STR model. Virtual corrections are accounted for using the ERT[26] calculations and the Sterman-Weinberg cutoffs ϵ and δ. The asymmetry, $A(\cos \chi)$, is shown in Fig. 39. The data have been corrected for all detector imperfections. However the effects of initial state radiation have not been corrected for in Fig. 39. The solid histogram is the prediction of either the IF and STR models which are indistinguishable. The solid line is perturbative QCD with $\alpha_s = 0.13$. Fits have been performed to the data for $|\cos \chi| < 0.72$ (where the fragmentation effects are minimized) and yield $\alpha_s(\text{STR}) = 0.14 \pm 0.01$ and $\alpha_s(\text{IF}) = 0.12 \pm 0.01$. Assuming an average $\alpha_s = 0.13 \pm 0.01 \pm 0.02$, the MARK J calculates $\Lambda(\overline{MS})$ using the second order formula given in Ref. 38 to be $\Lambda(\overline{MS}) = 180 {\textstyle +60 \atop \textstyle -40}$ MeV.

For the region $|\cos \chi| < 0.72$, the measurement is insensitive to large ranges of the cutoff parameter δ which was chosen to be 13° for this analysis. The α_s measurement is also insensitive to the choice of ϵ in the range $0.07 < \epsilon < 0.15$; $\epsilon = 0.1$ was used to obtain the results given above.

The CELLO group has performed a similar analysis with considerably less statistics than the MARK J. CELLO uses the LUND model to generate parton kinematics. For the IF model they turn off the effects of the string fragmentation and use instead Feynman-Field fragmentation. For the STR model, the standard LUND fragmentation model[8] is used. The virtual corrections are
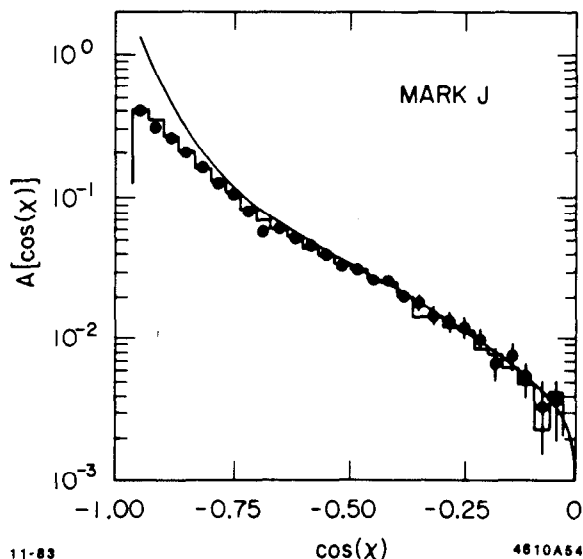

Fig. 39. Data from the MARK J for the energy-energy asymmetry compared with the prediction at the parton level with $\alpha_s = 0.13$. The histogram is the prediction of the two simulation models (STR and IF) which are indistinguishable in the plot.

39

implemented using the cutoff variable y_{ij} described earlier in this section. The results presented below are insensitive to the choice of a cutoff in y_{ij} in the range 0.017-0.05 which corresponds to a jet energy cutoff in the range 4.4-7.6 GeV. The CELLO group uses the variable χ instead of $\cos \chi$.

The CELLO asymmetry $A(\chi) = (1/\sin \chi)A(\cos \chi)$ is shown in Fig. 40. The predictions of the two Monte Carlo models are shown. The data is fit to the models in the region $\cos \chi < 0.92$ to yield the values $\alpha_s(\text{STR}) = 0.19 \pm 0.02$ and $\alpha_s(\text{IF}) = 0.12 \pm 0.02$.

The conclusion drawn by the CELLO group differs from that drawn by the MARK J; CELLO concludes that α_s determined using energy correlations is model dependent. It would be useful to compare the MARK J and CELLO data to see if the differences are in the data being fit or in the models used to fit the data. CELLO's data are fully corrected, but as discussed earlier the MARK J data are not corrected for the effects of initial state radiation. It would improve our understanding of the conflict if the MARK J could provide fully corrected data.

The MAC data are shown in Fig. 41. Their approach to the QCD model is the same as CELLO — they use the LUND generator with LUND fragmentation for STR and Feynman-Field fragmentation for IF. However MAC has not included
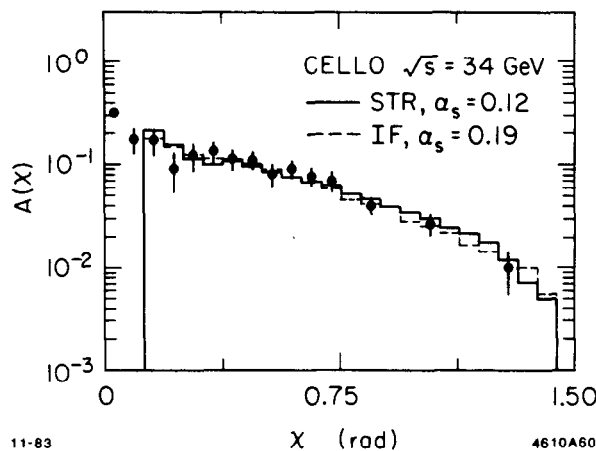

Fig. 40. The CELLO data for the asymmetry showing the predictions of the STR and IF models.
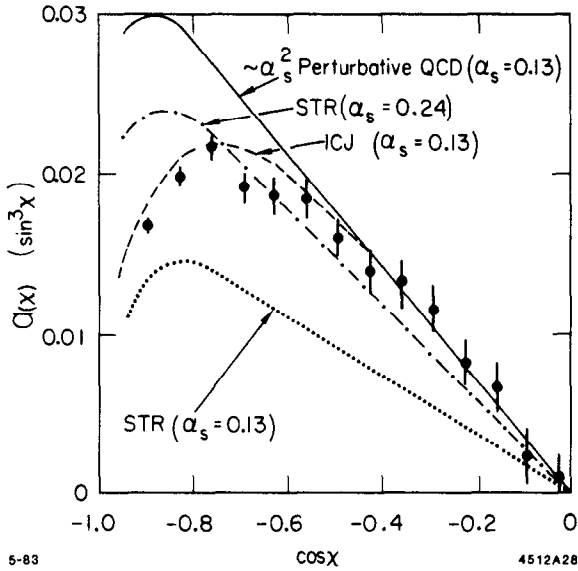
Fig. 41. The MAC asymmetry data showing the prediction at the parton level as well as predictions for the STR and IF models for various choices of α_s. Statistical errors are shown — systematics are $\pm 15\%$.

the effects of the virtual corrections. They present their analysis as a "status report" because they are struggling to understand the strong model dependence indicated by the curves in Fig. 41. The errors included in Fig. 41 are statistical only — the systematic errors are estimated to be $\sim 15\%$. The MAC data are fully corrected and can be compared directly with the CELLO data. This is done in Fig. 42. Unfortunately the CELLO data are statistics limited in the regions of $\cos \chi$ where fragmentation effects are minimized. However within the stated errors the data of CELLO and MAC agree where there is overlap.

Fig. 42. A comparison of the asymmetry as measured by MAC and CELLO.

41

The TASSO group has performed an analysis in which they choose groups of kinematic variables as "shape parameters" and then fit the data to the different Monte Carlo models. They make no distinction between two, three,... jet 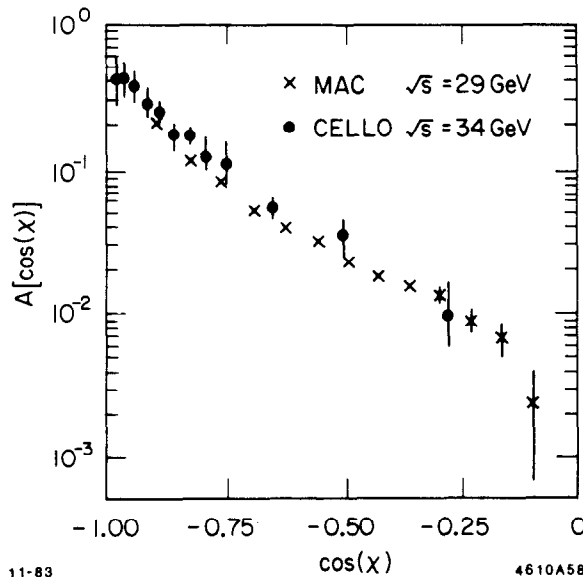topologies — all the hadronic events are used for the fits. The IF model is the Ali et al[24] generator with modified Feynman-Field fragmentation. The LUND Monte Carlo is used for the STR model. TASSO has fixed as many of the fragmentation parameters — $r = PS/V$, ϵ_c, ϵ_b, $P(s)/P(u)$, $P(q\bar{q})/P(q)$ — as they can using data from a variety of experiments. TASSO finds that a modification of the longitudinal fragmentation function for light quarks in the Feynman-Field model improves the quality of their fits. They use $f(z) = (1+a_L)(1-z)^{a_L}$ rather than the standard form $f(z) = 1 - a_L + 3a_L(1-z)^2$. For heavy quarks, TASSO uses the form given by Eq. (1). The distribution of the transverse momentum of the cascade partons is assumed to have the form $\exp(-q_T^2/2\sigma_q^2)$.

The virtual corrections are put in using the FKSS scheme[27] with Sterman-Weinberg cutoffs. The values of (ϵ, δ) used in this analysis are $(0.2, 40^o)$ which would correspond roughly to a cutoff in y_{ij} of 0.025 for a three parton state.

TASSO chooses variables for their fits which decouple as nearly as possible the fit parameters a_L, σ_q and α_s. The variables used are as follows:

(a) Jet mass. It has been stressed by Clavelli[39] that jet masses are a sensitive measure of gluon emission (α_s). Accordingly each event is divided into two hemispheres by a plane perpendicular to the sphericity axis. The mass of the particles in each of the hemispheres is calculated. Denoting the high (low) jet mass as M_H (M_L) the variable

$$\Delta M^2 = \frac{M_H^2 - M_L^2}{E_{vis}^2} \qquad \text{is formed.}$$

(b) The momentum tensor. The generalized momentum tensor is given by the formula

$$T_{\alpha\beta}^{(\gamma)} = \sum_j^N \frac{P_{j\alpha} P_{j\beta}}{(P_j)^{2-\gamma}} \bigg/ \sum_j^N |P_j|^\gamma$$

where α, β refer to the Cartesian momentum components of the jth particle and N denotes the number of particles in the event. Tensor $T^{(1)}$ and $T^{(2)}$ are used — $T^{(2)}$ corresponds to the familiar tensor associated with sphericity which has eigenvalues Q_1, Q_2 and Q_3. $T^{(2)}$ has the property that momentum enters quadratically. To avoid this quadratic dependence, $T^{(1)}$ with its eigenvalues L_1, L_2 and L_3, is employed. The role of the L_j is analogous to the role of the more familiar Q_j.

(c) $x_p = 2p/\sqrt{s}$, p_T^{out}, p_T^{in}. Here p_T^{out} (p_T^{in}) measure the amount of momentum out of (in) the event plane where the event plane is defined by the $T^{(2)}$ analysis (sphericity).

For a given model a lattice of $5 \times 5 \times 5$ points in the a_L, σ_q, α_s space was used. 2000 Monte Carlo events were generated for each lattice point and the contents of each bin of each distribution was parametrized by a second order polynomial in a_L, σ_q and α_s. These parametrizations were then fit to the corrected data to yield fit values. The results are summarized in Table 6 for the STR and IF models. The fitted distribution columns are most sensitive to a_L, σ_q and α_s respectively. The contribution to the overall χ^2 is shown for each variable separately. The variables in column three, which determine the value of α_s most directly, have reasonable χ^2 contributions — namely these distributions are well fit. Only statistical errors have been used here; the addition of systematic errors in the quantity x_p for instance will reduce it χ^2 contribution to a reasonable

Table 6(a). TASSO fit results for the independent jet model, second order
QCD (IF)

Distribution (χ^2/DF)			Overall χ^2/DF	a_L	σ_q	α_s
$x_p(4.6)$	$Q_1(2.3)$	$Q_2(1.9)$	3.6	$.687 \pm .017$	$.362 \pm .003$	$.166 \pm .003$
$x_p(\ )$	$p_{Tout}(3.3)$	$p_{Tin}(1.9)$	4.8	$.639 \pm .014$	$.350 \pm .002$	$.155 \pm .002$
$x_p(\ )$	$L_1(1.6)$	$L_2(1.9)$	3.8	$.697 \pm .016$	$.346 \pm .003$	$.155 \pm .003$
$x_p(4.7)$	$Q_1(2.0)$	$\Delta M^2(0.7)$	3.3	$.678 \pm .020$	$.355 \pm .003$	$.166 \pm .004$

Table 6(b). TASSO fit results for the String model, second order QCD (STR)

Distribution (χ^2/DF)			Overall χ^2/DF	a_L	σ_q	α_s
$x_p(4.0)$	$Q_1(2.8)$	$Q_2(1.2)$	3.2	$.449 \pm .017$	$.362 \pm .004$	$.216 \pm .003$
$x_p(\ )$	$p_{Tout}(5.2)$	$p_{Tin}(2.5)$	4.0	$.473 \pm .012$	$.324 \pm .003$	$.201 \pm .003$
$x_p(\ )$	$L_1(8.8)$	$L_2(2.2)$	4.9	$.390 \pm .016$	$.323 \pm .004$	$.221 \pm .003$
$x_p(4.0)$	$Q_1(2.8)$	$\Delta M^2(1.1)$	3.2	$.437 \pm .020$	$.320 \pm .004$	$.219 \pm .004$

level. The most notable result from Table 6 for our discussion here is that for the STR model $\alpha_s \approx 0.21$ whereas for the IF model $\alpha_s \approx 0.16$.

The TASSO group has shown that if a kinematic region is chosen for the variables Q_2, p_T^{in}, L_2 and ΔM^2 which strongly enhances the perturbative process (3 jet events), the values obtained for α_s are almost identical to those obtained by the fits to the full kinematic range. If the Sterman-Weinberg cutoff parameters (ϵ, δ) are varied from $(0.175, 35^o)$ to $(0.255, 45^o)$, α_s changes by +0.02 in both models.

The TASSO analysis indicates that there is a significant model dependence in the determination of α_s.

For completeness we can state the published result of the JADE group[32] which used a fit to three jet event topologies to make the second order α_s determination $\alpha_s = 0.160 \pm 0.015 \pm 0.030$ where the result is independent of the fragmentation model used within the stated errors.

What should we conclude then about these measurements of α_s? This reviewer would make the following observations:

(a) Different analysis procedures encounter different problems. However they all rely on the use of models to obtain a measurement of α_s.

(b) The measurements of α_s are model dependent and could be procedure dependent.

(c) With the strong dependence on models it would be useful if the Monte Carlo simulation programs could be kept more uniform. With all the groups using different parameters and different fragmentation models and different second order cutoff procedures, comparisons between results, especially when they reach different conclusions, are difficult.

(d) We must remember that the STR and IF models represent two different extremes with respect to the application of color strings. The real world probably lies somewhere in between. In addition, neither model includes the effects of soft gluons — these could still be important at these energies.

(e) Patience is a virtue — what seems to be a cloudy situation now might well become clearer in the future — so we should not get too upset by the present difficulties with the α_s determination. In particular if PETRA could get a reasonable sized data set at high energy ($\sqrt{s} >$ 40 GeV), this will help the situation considerably. In particular one could then measure the energy dependent effects which we are now trying to model.

(b) Transverse Momentum Structure of Jets in the Energy Range 9 – 32 GeV

The PLUTO group has made a very thorough study of the P_t structure of particles in jets in the energy range 9.4-31.6 GeV. All their data are fully corrected for detector and initial state radiation effects. Comparisons are made with the leading log QCD (LLA) predictions of Rakow and Webber[40]. The reason for making a comparison with LLA calculations is that they include the effects of soft gluons. Figure 43(a) shows the evolution of $\langle \sum_i P_t^i \rangle / \sqrt{s}$ with $\sqrt{s}$. The sum ranges over all the charged and neutral particles and P_t is measured with respect to the thrust or sphericity axis. The average is taken over all the events. The fit shown in Fig. 43(a) is to the LLA prediction of Rakow and Webber and it yields a value of $\Lambda = 600 \pm 25$ MeV which would correspond to $\alpha_s(900 \text{ GeV}^2) = 0.20 \pm 0.01$. Reference to different jet axes yields a systematic effect of 0.01 in α_s. PLUTO has studied the effects of fragmentation on the determination of α_s. If they use their simulation program to study the difference between the average P_t as measured by the primary vector and pseudoscalar mesons rather than by their decay products, they find that α_s is 25% lower. Hence they conclude that, while the Rakow and Webber LLA prediction fits the evolution of the average P_t very well, fragmentation effects preclude an accurate determination of α_s.
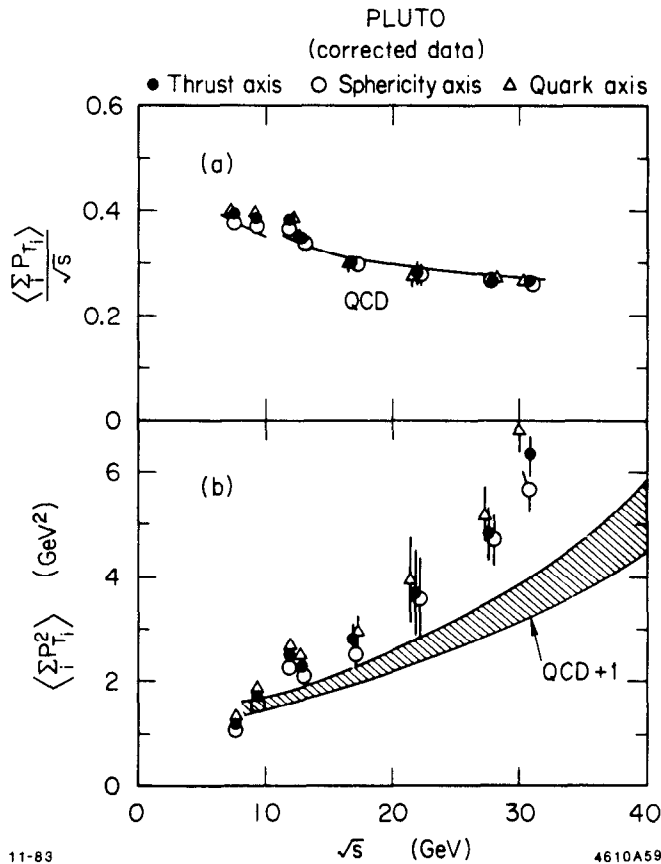

Fig. 43. The PLUTO data for (a) $\langle \sum P_t \rangle / \sqrt{s}$ as a function of $\sqrt{s}$. The full (open) circles refer to P_t relative to the thrust (sphericity axis). The triangles refer to values of P_t obtained with respect to the most energetic parton direction. The solid line indicates the LLA QCD prediction of Rakow and Webber for $\Lambda = 600$ MeV. (b) $\langle \sum P_t^2 \rangle$ as a function of $\sqrt{s}$. The prediction of Rakow and Webber is represented by the shaded area.

45

Figure 43(b) shows the evolution of the average P_t^2. In this case the prediction of Rakow and Webber does not account well for the data and the discrepancy cannot be explained by fragmentation effects.

(c) Does the Gluon Fragment Differently Than the Quark?

There has been evidence from the JADE group[41] that the transverse momentum which characterizes the fragmentation of a gluon is different than that for quarks. This evidence was based on their data at $\sqrt{s} > 29$ GeV. JADE has now added to their analysis the data for $\sqrt{s} = 22$ GeV and expanded the scope of their analysis. Their conclusion remains that gluon enriched jets exhibit larger $\langle P_t \rangle$ in their fragmentation. We present here some of the arguments and comment on the analysis.

A sphericity analysis was performed on the data and cuts ($Q_1 < 0.06$, $Q_2 - Q_1 > 0.07$) are made to select planar, 3 jet events. Particles in these planar events were assigned to one of three jets using the method of triplicity.[42] The jet directions were then calculated from the vector sum of the particles which constitute each jet. Because jet directions are better measured than jet energies, the jet energies are calculated from the jet directions on the assumption that the partons are massless. These energies, E_j^d, were then ordered such that $E_1^d > E_2^d > E_3^d$. Events having a jet with less than four particles or an observed energy of less than 2 GeV were removed from the sample. Both charged and neutral particles were used in the analysis. At 33 GeV the Monte Carlo models for QCD indicate that the probabilities that jet #1, #2 and #3 is the gluon are 12, 22 and 51% respectively and 9, 20 and 34% at 22 GeV. The sum of these three probabilities is not 100% because the 3 jet sample is contaminated by $q\bar{q}$ events. The thrust of the analysis now is to compare jets of the same energy but with different gluon content.

Figure 44(a) shows the $\langle P_t \rangle$ measured relative to the jet axes for the three jets. Data are from the 22 and 33 GeV energy regions. The data are not corrected for detector biases, and both neutral and changed tracks enter into the plot. Jet #2 has a smaller $\langle P_t \rangle$ than jet #3. The Monte Carlo models predict that the gluon content of jet #2 is $\sim 25\%$ and that of jet #3 is $\sim 50\%$ for $6 < E_{2,3}^d < 10$ GeV. The data in this jet energy region are plotted in Fig. 45 in terms of P_t. In the region of 0.2 GeV/c $< P_t < 1.5$ GeV/c the data were fit with $d\sigma/dP_t \propto exp(-A_j P_t)$ and the ratio of $A_2/A_3 = 1.13 \pm 0.04$ was found indicating that the jet with higher gluon content has a larger $\langle P_t \rangle$. Using charged particles only $A_2/A_3 = 1.10 \pm 0.05$.

We return now to Figs. 44(b)-(d). Two models were used for comparison with the data. The result of the LUND model is shown in Fig. 44(d). The

model used in Figs. 44(b) and 44(c) is the independent fragmentation model of Hoyer et al.[25] In Fig. 44(b) the quarks and gluons fragment identically, namely $\sigma_q = \sigma_g = 330$ MeV/c, whereas in Fig. 44(c) $\sigma_q = 330$ MeV/c but $\sigma_g = 500$ MeV/c — the gluon is assigned a larger primordial P_t.

At the heart of this test is the question of whether QCD is a non-Abelian theory. If it is, then the presence of a gluon self coupling term would in fact provide a broader P_t for gluon jets than for quark jets of the same energy. So JADE is probing a very important question here and their result could prove to be very significant. For such an important issue it would be comforting to have confirmation — such confirmation is still not forthcoming. It is unfortunate that the JADE test hinges so crucially on the models for its result. The author has concerns about the procedure (any procedure at these energies) of assigning particles to jets #2 and #3. Because of the proximity of these two jets, there will be a tendency to assign some particles to the wrong jet. In particular, jet #3 is looking for ways to get over the definition cuts of low multiplicity and energy discussed earlier. The misassigned particles will tend to have larger than average P_t. The JADE response to this criticism would be that the application of the LUND model or the independent fragmentation model with $\sigma_g > \sigma_q$ reproduces the data (Fig. 44). Hence the comment that the result hinges on the models. Inadequacies in the models could possibly contribute to an incorrect conclusion.

(d) Can We Distinguish Experimentally the Difference Between the String Picture and the Independent Fragmentation Picture?

We have indicated in this section that the determination of α_s is model dependent and in particular one obtains a different value for α_s using the string model and the independent fragmentation model. An obvious question then is can we determine whether one of these models provides a more accurate representation of the data? The JADE group has presented several ways of looking at this problem — we choose one here for illustration. Again the three jet (planar) events are used (see Section c). For each particle the transverse momentum is calculated in the event plane relative to the reconstructed jet axis (P_t^{in}) where the sign of P_t^{in} is defined by the insert in Fig. 46(a). Figure 46 shows $\langle P_t^{in} \rangle$ plotted against $P_{\|}$, where $P_{\|}$ is the momentum component along the jet axis. Also shown on the figure are the predictions of the LUND model and the Hoyer et al. model, where the models have been optimized for the total data set. The data favor the LUND description. However, we have to ask ourselves whether we are testing something fundamental about the difference between the string picture and nonstring picture or whether we are measuring differences and/or inadequencies in the models used in the analysis? The author has concerns about tests which depend so strongly on the simulation models for their interpretation.
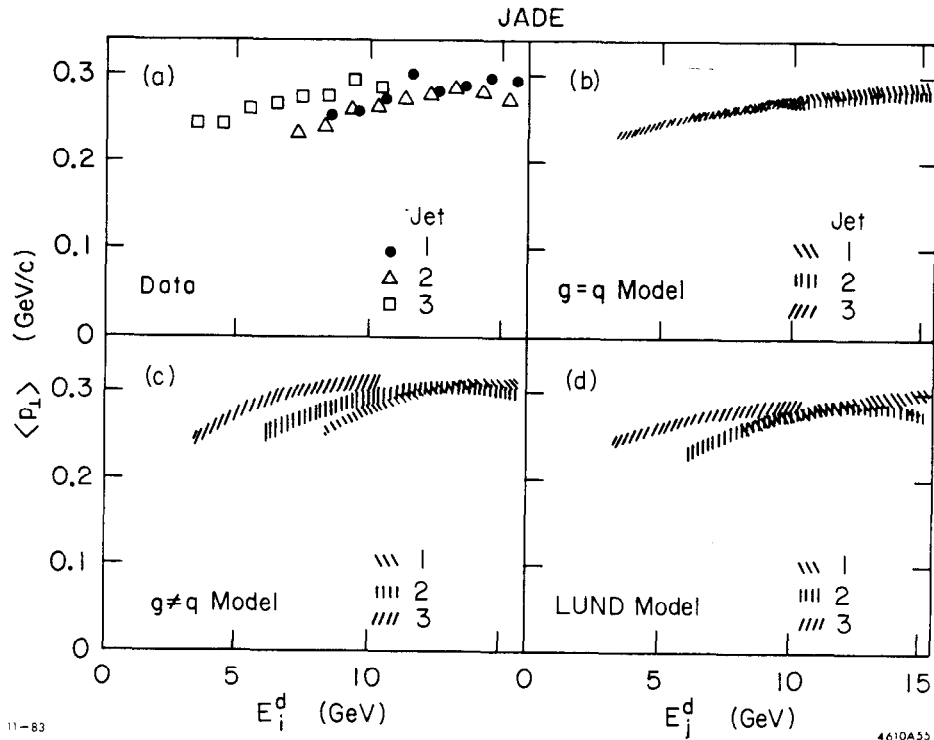
Fig. 44. The JADE measurement of $\langle P_t \rangle$ as a function of jet energy for particles in three jet events. (a) Data from $\sqrt{s} = 22$ and 33 GeV, (b) prediction of the Hoyer model with identical quark and gluon fragmentation, (c) prediction of the Hoyer model with broader P_t for gluon fragmentation relative to quark and (d) prediction of the LUND model.
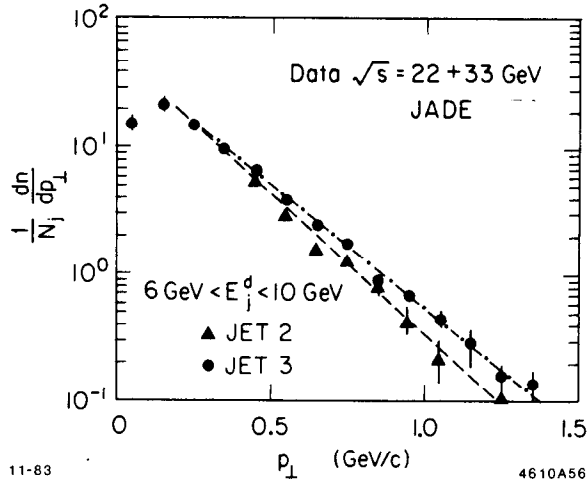
48

Fig. 45. The normalized differential cross section as a function of P_t for JADE data at $\sqrt{s} = 22$ and 33 GeV. Data are shown for the low and intermediate energy jet.
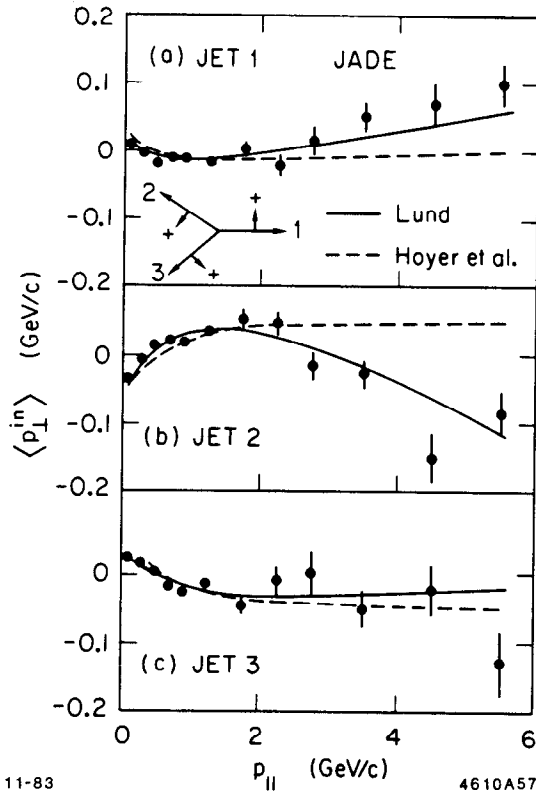

Fig. 46. JADE data for P_t^{in} as a function of $P_\parallel$ for particles in three jet events. The predictions of the LUND and Hoyer models are shown.

49

(e) Baryon, Charge and Jet Mass Correlations; KNO Scaling

Is baryon number conserved locally in a jet or globally in an event? The TASSO group has presented evidence that baryon number compensation in the $\sqrt{s} = 34$ GeV region is mostly a local phenomenon. They consider hadronic events with pp, $p\bar{p}$ and $\bar{p}\bar{p}$ topologies, requiring $p > 1$ GeV/c for the baryons. Using their Cherenkov counters, TASSO is able to identify protons with momenta up to the maximum allowed kinematically. They classify the dibaryon events according to whether the baryons are in the same jet or in opposite hemisphere jets. The results are shown in Table 7. Contributions from background topologies have been subtracted but the entries are not corrected for detector inefficiencies. The entries in Table 7 are numbers of events. One sees that the TASSO data imply that for fast baryons, the baryon number compensation occurs mostly in the same jet, i.e. is a local phenomenon. However more statistics are needed to see if there is any long range compensation. In a contribution to this conference, A. Bartl et al.[43] predict a 10-20% compensation in opposite jets at this $\sqrt{s}$.

Table 7. TASSO baryon correlations. Background
subtracted event populations are shown.

	Same Jet	Opposite Jet
$pp + \bar{p}\bar{p}$	-0.2 ± 2.1	2.7 ± 3.1
$p\bar{p}$	15.0 ± 4.6	3.0 ± 3.0

The HRS and TPC groups have looked into the correlations of charged multiplicity. The hadronic events are divided into two hemispheres (forward and backward) by a plane perpendicular to the sphericity axis — cuts on event shape are made to select predominantly two jet events. The TPC data are shown in Fig. 47 where the average charged multiplicity in the backward hemisphere is plotted as a function of the multiplicity in the forward hemisphere. [The variable $y = (1/2)\ln(E + P_{\parallel}/E - P_{\parallel})$ is the rapidity.] The curve is the prediction of the LUND Monte Carlo. The TPC sees no large charge multiplicity correlations — those exhibited in the plot are due to instrumental effects of solid angle coverage and hadron selection criteria (charged multiplicity > 5). The HRS data are shown in Fig. 48 for two regions of rapidity. In Fig. 48(b) the central region is removed. The HRS data, like those of TPC, support the fragmentation independence of the two jets. The dotted line in Fig. 48(a) represents the trend of the central region of 540 $p\bar{p}$ data.[44] The HRS has also looked into jet mass correlations as shown in Fig. 49. They support the results of the charged

multiplicity, namely there is no evidence for large correlations between the two fragmenting jets.

HRS has studied KNO scaling.[45] Their data are shown in Fig. 50 as compared to data from $p\bar{p}$ annihilation and pp interactions. The HRS e^+e^- data are clearly narrower. However their result is in reasonable agreement with the TASSO data.[46]
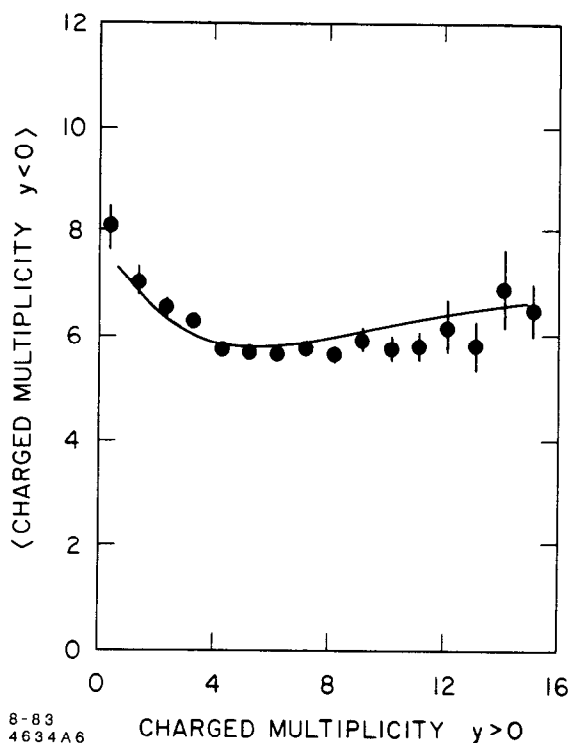

8-83
4634A6   CHARGED MULTIPLICITY   y > 0

Fig. 47. TPC data for multiplicity correlations. The apparent correlation is an artifact of the detector and analysis cuts as shown by the Monte Carlo prediction.
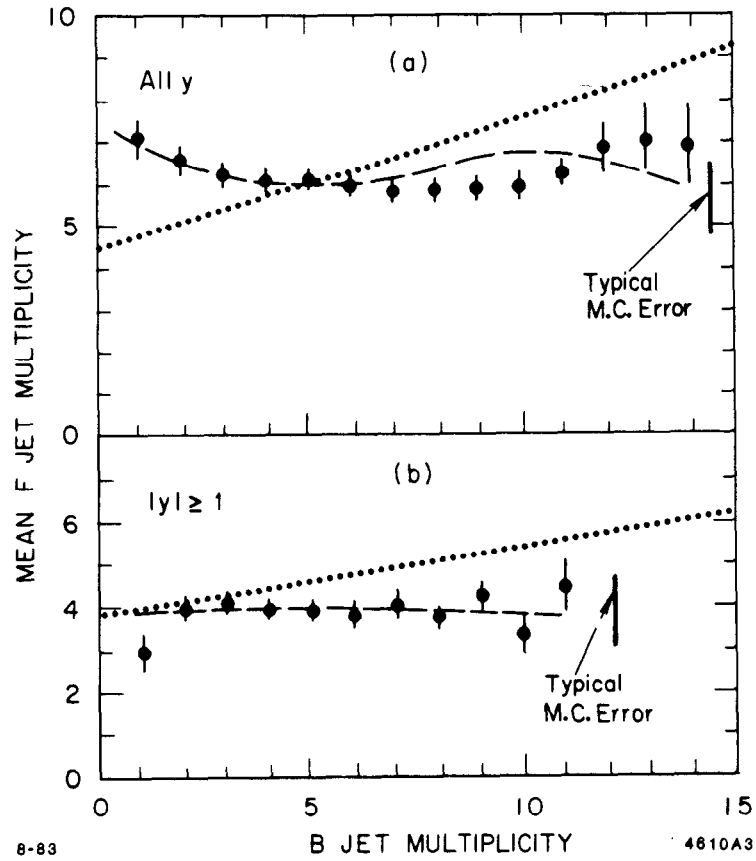
Fig. 48. HRS data for multiplicity correlations for (a) all
the data and (b) the central region $|y| \leq 1$ is removed.
The dashed line is the prediction of the Monte Carlo
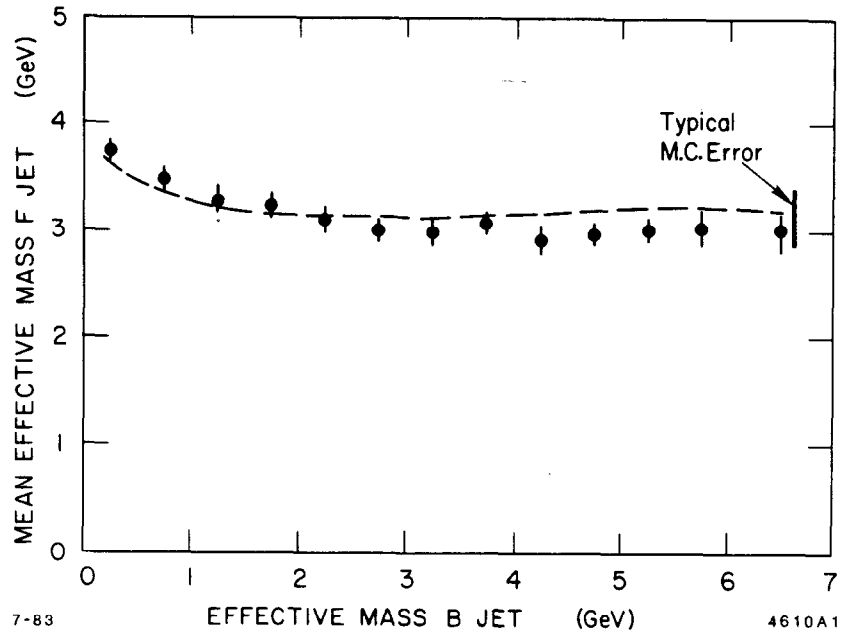and the trend of the 540 GeV $\bar{p}\,p$ data is indicated as a
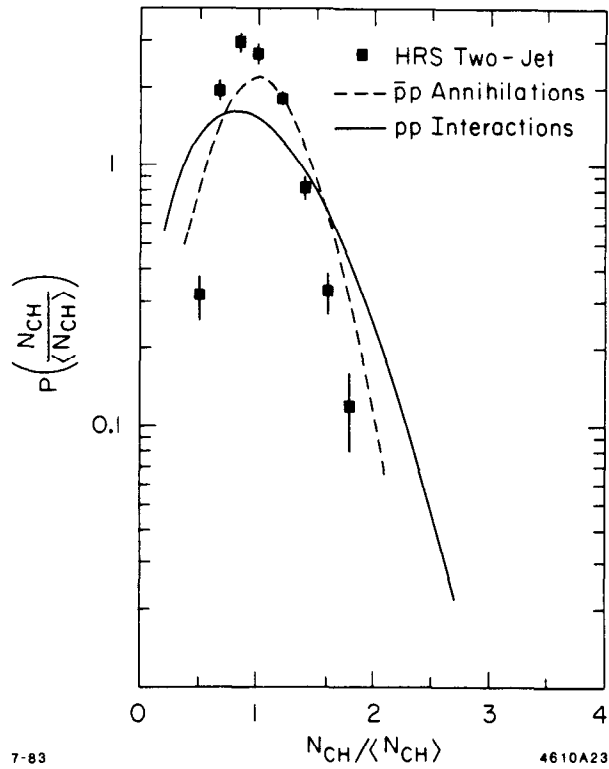dotted line.

Fig. 49. HRS data for jet mass correlations.

Fig. 50. KNO multiplicity distribution for the HRS two jet events compared to pp and $\bar{p}p$ data.

4. ACKNOWLEDGEMENTS

5. REFERENCES AND FOOTNOTES

1. M. Althoff *et al.*, Z. Phys. C17, 5 (1983).

2. For a description of the TPC detector, see John Hadley, LBL-16116 (Ph.D. Thesis).

3. For a description of the DELCO detector, see J. Kirkby, Proceedings of the XXI International Conference on High Energy Physics, Paris, France, 1982, p. C3-45.

4. H. Behrend *et al.*, DESY 83-066 (1983).

5. D. L. Scharre *et al.*, Phys. Rev. Lett. 41, 1005 (1978).

6. R. Brandelik *et al.*, Phys. Lett. 108B, 71 (1982).

7. W. Bartel *et al.*, DESY 83-063 (1983).

8. T. Sjostrand, Comp. Sci. Comm. 27, 243 (1982); T. Sjostrand, Comp. Sci. Comm. 28, 229 (1983); B. Anderson *et al.*, Z. Phys. C6, 235 (1980); Nucl. Phys. B197, 45 (1982).

9. R. Brandelik *et al.*, Phys. Lett. 117B, 135 (1982).

10. See for instance, Sau Lan Wu, DESY 83-007 (1983).

11. W. Bartel *et al.*, DESY 83-042 (1983).

12. M. Althoff *et al.*, DESY 83-071 (1983).

13. For a description of the CLEO detector, see D. Andrews *et al.*, Nucl. Instrum. Methods 211, 47 (1983).

14. G. H. Trilling, Proceedings of the XXI International Conference on High Energy Physics, Paris, France, 1982, p. C3-57.

15. M. Althoff *et al.*, DESY 83-010 (1983).

16. C. Peterson *et al.*, Phys. Rev. D 27, 105 (1983).

17. P. Avery *et al.*, CLNS 83/574 (1983).

18. It should be noted that all D^* results quoted in this paper use the branching fraction for $D^{*\pm} \rightarrow D^o\pi^\pm$ of 0.44 ± 0.10 except for the CLEO results. CLEO uses the value 0.60 ± 0.15 and hence comparisons should be made with some care.

19. M. E. Nelson *et al.*, Phys. Rev. Lett. 50, 1542 (1983).

20. E. Fernandez *et al.*, Phys. Rev. Lett. 50, 2054 (1983).

21. B. Adeva *et al.*, Phys. Rev. Lett. 51, 443 (1983).

22. QCD Tests at the Υ were covered by other speakers.

23. Certainly there are more models available as programs and in the literature. We choose here to describe the models which have been used in the analyses of α_s. A paper discussing an alternative model was submitted to this conference: The Hypothesis of Statistical Jet Evolution Confronted with e^+e^- Annihilation Data — W. Ochs, MPI-PAE/EXP El 118 (C-228).

24. A. Ali *et al.*, Phys. Lett. 93B, 155 (1980).

25. P. Hoyer *et al.*, Nucl. Phys. B161, 349 (1979).

26. R. K. Ellis *et al.*, Nucl. Phys. B178, 421 (1981); J. Vermasseren *et al.*, Nucl. Phys. B187, 301 (1981).

27. K. Fabricius *et al.*, Phys. Lett. 97B, 431 (1980).

28. T. Gottschalk, Phys. Lett. 109B, 331 (1982).

29. G. Sterman and S. Weinberg, Phys. Rev. Lett. 39, 1436 (1977).

30. R. D. Field and R. R. Feynman, Nucl. Phys. B136, 1 (1978).

31. B. Adeva *et al.*, Phys. Rev. Lett. 50, 2051 (1983).

32. W. Bartel *et al.*, Phys. Lett. 119B, 239 (1982).

33. Yu. L. Dokshister *et al.*, Phys. Lett. 78B, 290 (1978); C. L. Basham *et al.*, Phys. Rev. Lett. 41, 1585 (1978); Phys. Rev. D 19, 2018 (1979).

34. Ch. Berger *et al.*, Phys. Lett. 99B, 292 (1981).

35. D. Schlatter *et al.*, Phys. Rev. Lett. 49, 521 (1982).

36. H. J. Behrend *et al.*, DESY 82-061 (1982).

37. S. Ellis, Phys. Lett. 117B, 333 (1982).

38. A. Ali and F. Barreiro, Phys. Lett. 118B, 155 (1982).

39. L. Clavelli, contribution to this conference (C-240), ANL-HEP-CP-83-05, provides the motivation for the use of this variable.

40. P. E. L. Rakow and B. R. Webber, Nucl. Phys. B191, 83 (1981).

41. W. Bartel *et al.*, Phys. Lett. 123B, 460 (1983).

42. S. Brandt and H. Dahmen, Z. Phys. C1, 61 (1979).

43. A. Bartl, H. Fraas, H. R. Gerhold and W. Majirotto, Influence of Baryon Production on Charge Distributions of Jets (C-61).

44. K. Alpgard *et al.*, Phys. Lett. 123B, 361 (1983).

45. Z. Kobe *et al.*, Nucl. Phys. B40, 317 (1972).

46. See for instance, G. Wolf, DESY 81-086 (1981).